Chemical Geology 572 (2021) 120198

Contents lists available at ScienceDirect

Chemical Geology

journal homepage: www.elsevier.com/locate/chemgeo

Precise U—Pb dating of grandite garnets by LA-ICP-MS: Assessing ablation behaviors under matrix-matched and non-matrix-matched conditions and applications to various skarn deposits

Ying-Hua Chen [a,b], Rui-Zhong Hu [a,b,*], Ting-Guang Lan [a,b,*], Hong Wang [a,b], Yan-Wen Tang [a], Yue-Heng Yang [c], Zhen-Dong Tian [a,b], Thomas Ulrich [d]

[a] State Key Laboratory of Ore Deposit Geochemistry, Institute of Geochemistry, Chinese Academy of Sciences, Guiyang 550081, China
[b] College of Earth and Planetary Sciences, University of Chinese Academy of Sciences, Beijing 100049, China
[c] State Key Laboratory of Lithospheric Evolution, Institute of Geology and Geophysics, Chinese Academy of Sciences, Beijing, 100029, China
[d] Institute for Geosciences, Aarhus University, Aarhus, 8000, Denmark

ARTICLE INFO

Editor name: Dr. Balz Kamber

Keywords:
Grandite garnet
LA-ICP-MS U—Pb dating
U-Pb fractionation
Matrix effect
Ablation parameter

ABSTRACT

LA-ICP-MS U—Pb dating of garnet has become one of the important geochronometric methods in recent years. Both the matrix-matched and non-matrix-matched external standards were used for dating. However, under which conditions reliable ages can be obtained and the difference between the matrix-matched and non-matrix-matched methods have not been well constrained. In this contribution, a series of ablation experiments (including spot analysis and line scanning) were conducted on different grandite garnets using various ablation parameters (spot size, repetition rate and fluence) under both the matrix-matched (garnet as external standard) and non-matrix-matched (zircon as external standard) conditions, with the aim to obtain the optimal conditions for precise LA-ICP-MS garnet U—Pb dating. The results show that U—Pb fractionation associated with downhole depth, intrinsic properties of U (more refractory) and Pb (more volatile) and radiation damage (alpha dose) of crystal lattice occurs in zircon and garnet. The fractionation can be minimized or even eliminated by optimizing the ablation parameters (e.g., large spot size and low repetition rate) or the analytical modes (e.g., line scanning). This makes it feasible to use zircon as external standard for garnet U—Pb dating. Line scanning is most favorable for garnet U—Pb dating at broad ablation parameters regardless of matrix-matched or non-matrix-matched. In spot analysis mode, all the garnets can be precisely dated using a large spot size (e.g., ≥90 μm) coupled with moderate-low repetition rate (e.g., 2–5 J/cm^2) and fluence (e.g., 2–5 J/cm^2) under matrix-matched condition. Under non-matrix-matched condition, all the garnets can also be precisely dated when a larger spot size (e.g., ≥120 μm) coupled with moderate repetition rate (e.g., 5 Hz) and fluence (e.g., 5 J/cm^2) is used. Too high or too low repetition rates (e.g., <2 Hz and > 10 Hz) and fluences (e.g., <2 J/cm^2 and > 10 J/cm^2) were found to be unsuitable for garnet U—Pb dating. Low-U and high-U samples are best treated differently due to their different U—Pb fractionation coefficients, especially at the high fluence and repetition rate conditions. Equally, U-concentration matched garnet standards are required to improve the accuracy and precision of the U—Pb dating

Natural grandite garnets selected from Fe, W and Cu—Mo skarn deposits can be precisely dated using the optimized methods. These garnets have compositions varying widely between andradite and grossular with variable U (1–100 ppm) and common Pb (f_{206} of 0–0.7) concentrations, indicating that the methods are reliable and thus suitable for wide applications.

1. Introduction

Grandite garnets are a solid-solution series of andradite ($Ca_3Fe_2Si_3O_{12}$) and grossular ($Ca_3Al_2Si_3O_{12}$), which occur in a variety of magmatic intrusions (Huggins et al., 1977; Barrie, 1990; Scheibner et al., 2007; Python et al., 2007) and calc-silicate skarns typically associated with economic Fe, Cu, W, Sn and Mo deposits (Smith et al., 2004; Meinert et al., 2005; Xu et al., 2016). They have long been used for

* Corresponding authors at: Institute of Geochemistry, Chinese Academy of Sciences, No.99 Linchengxi Road, Guiyang, Guizhou Province 550081, China.
E-mail addresses: huruizhong@mail.gyig.ac.cn (R.-Z. Hu), lantingguang@126.com (T.-G. Lan).

https://doi.org/10.1016/j.chemgeo.2021.120198
Received 30 April 2020; Received in revised form 23 March 2021; Accepted 25 March 2021
Available online 27 March 2021

Table 1
Summary of the reference materials and the garnet samples.

Sample	Description	Composition	U (ppm)	Th (ppm)	Sm (ppm)	Age (Ma)	Source
Reference zircon or garnet							
91500	Zircon	$ZrSiO_4$	70–100, mean of 80	28–35, mean of 30	0.2–0.6, mean of 0.4	1065.4 ± 0.3 (TIMS)	Wiedenbeck et al. (2004)
Willsboro	Skarn, yellow	$And_{90}Grs_{10}$	1.0 ± 0.5 (2SD)	0.8 ± 0.5 (2SD)	1.2–2.4, mean of 1.8	1022 ± 16 (TIMS)	Seman et al. (2017)
Mali	Probably skarn, red	$And_{52}Grs_{37}$	7.0 ± 6.8 (2SD)	3.3 ± 6.8 (2SD)		202.0 ± 1.2 (TIMS)	Seman et al. (2017)
QC04	Skarn, dark-red	$And_{90\text{-}98}Grs_{1\text{–}8}$	38–130, mean of 76	0.1–3.0, mean of 1.6	0.1–1.4, mean of 0.6	130.0 ± 1.0 (LA-ICP-MS)	Deng et al. (2017)
Jinling Fe skarn deposit (36°51′ N, 118°10′ E)							
ZB23	Endoskarn, dark-red	$And_{72}Grs_{28}$	10.2–20.0, mean of 14.4	1.2–11.2, mean of 3.5	23–66, mean of 40	129.6 ± 0.8 (LA-ICP-MS)	This study
ZB05	Exoskarn, red-brown	$And_{94}Grs_{6}$	6.1–14.3, mean of 9.6	0.1–0.4, mean of 0.2	0.01–0.5, mean of 0.1	129.6 ± 0.3 (LA-ICP-MS)	This study
ZB03	Exoskarn, oscillatory zoning, yellow	$And_{54\text{-}98}Grs_{2\text{–}47}$	1.1–4.3, mean of 2.6	0.1–8.6, mean of 2.5	0.1–5.7, mean of 1.8	129.3 ± 1.2 (LA-ICP-MS)	This study
Xintianling W skarn deposit (25°39′ N , 112°57′ E)							
XTL01	Skarn, oscillatory zoning, red-brown	$And_{31\text{-}75}Grs_{22\text{–}64}Sp_{2\text{–}6}$	3.2–21.6, mean of 7.6	0.1–2.5, mean of 0.5	0.5–1.9, mean of 1.0	158.2 ± 0.5 (LA-ICP-MS)	This study
XTL02	Skarn, red-brown	$And_{45\text{-}60}Grs_{34\text{-}47}Sp_{6\text{–}9}$	6.1–19.5, mean of 12.9	0.1–0.8, mean of 0.3	0.6–1.8, mean of 1.2	158.1 ± 0.9 (LA-ICP-MS)	This study
Hongshan Cu—Mo skarn deposit							
Hongshan	Exoskarn, dark-red	$And_{40\text{-}61}Grs_{37\text{–}57}$	15–38, mean of 23	0.01–0.9, mean of 0.3	4.2–12.3, mean of 7.5	80.7 ± 0.4 (LA-ICP-MS)	Tian et al. (2019)

U—Pb, Lu—Hf and Sm—Nd geochronology based on ID-TIMS (isotope dilution–thermal ionization mass spectrometry) or MC-ICP-MS (multi collector-inductively coupled plasma-mass spectrometry) analysis after chemical digestion and separation (Mezger et al., 1989; Scherer et al., 2000; Jung and Mezger, 2003; Smit et al., 2013; Cheng et al., 2018; Jung et al., 2019). The above analytical methods, however, have drawbacks of inclusion interference, time-consuming and costly. Recently, grandite garnets were applied for LA-ICP-MS (laser ablation-inductively coupled plasma-mass spectrometry) U—Pb dating because they contain relatively high U concentrations (several to hundreds of ppm U) compared with other garnets (Deng et al., 2017; Seman et al., 2017; Gevedon et al., 2018; Yan et al., 2020). The precision of the LA-ICP-MS garnet U—Pb dating is 1–10% when using matrix-matched external standard for correction (Seman et al., 2017). Interestingly, other studies showed that non-matrix-matched external standards such as zircon standards (e.g., 91500 and GJ-1) can also be applied for the garnet U—Pb dating (Deng et al., 2017; Li et al., 2018; Wafforn et al., 2018; Zhang et al., 2019; Fan et al., 2021). If it is true, the method has excellent potentials for wide applications because garnet standards are not always available but zircon standards are ubiquitous. However, so far, under which conditions reliable ages can be obtained from the non-matrix-matched analysis and the difference between the matrix-matched and non-matrix-matched methods have not been well constrained. It is thus necessary to investigate the ablation behaviors of granite garnets and the associated U—Pb fractionation under both the matrix-matched and non-matrix-matched conditions. This would greatly promote the understandings of the garnet U—Pb geochronology.

Uranium incorporation into grandite garnets is mainly associated with the coupled substitution for major elements (e.g., Ca, Fe, Al and Si, Smith et al., 2004; Gaspar et al., 2008; Deng et al., 2017; Zhang et al., 2019), the concentrations of which are thus highly dependent on the compositions of the garnets. This implies that matrix effect might be a major factor affecting the LA-ICP-MS U—Pb dating. In addition, grandite garnets commonly incorporate variable common Pb during their growth (Deng et al., 2017; Seman et al., 2017), which need to be corrected with the highest accuracy to minimize the uncertainty of the U—Pb age (El Korh, 2014). This suggests that an appropriate correction strategy for common Pb is required.

Previous studies showed that matrix effect and elemental fractionation during LA-ICP-MS analysis can be minimized by optimizing the analytical conditions, such as adding water vapor before the ablation cell (Luo et al., 2018, 2019), using active laser focusing (Hirata and Nesbitt, 1995), soft (Hirata, 1997) or linear ablation (Li et al., 2001) and changing the ablation parameters of laser fluence, spot size, repetition rate and carrier gas flow (Horn et al., 2000; Poitrasson et al., 2003; Shaheen et al., 2012; Thompson et al., 2018). For the garnet U—Pb dating, available studies showed that large spot sizes and high repetition rates seem to work well (Seman et al., 2017; Yang et al., 2018; Burisch et al., 2019; Bineli Betsi et al., 2020). In this study, in combination with appropriate initial Pb correction strategies, a series of ablation experiments (spot analysis and line scanning) were conducted on different grandite garnets using various ablation parameters (spot size, repetition rate and laser fluence) under both the matrix-matched (garnet as external standard) and non-matrix-matched (zircon as external standard) conditions. The laser-induced U—Pb fractionation between garnet and zircon as well as among garnets was investigated and the mechanisms were discussed. The optimal parameters for precise garnet U—Pb dating under different conditions (especially for high-U and low-U garnets, respectively) were obtained. The optimized methods were finally applied to various skarn deposits to test their validity and usefulness. The garnet U—Pb dating is typically meaningful for skarn deposits due to the garnets ubiquitous in both the magmatic and hydrothermal stages (Deng et al., 2017), facilitating to decipher the magmatic-hydrothermal processes in this type of mineralization.

2. Reference materials and garnet samples

2.1. Reference materials

Three garnet reference materials (Willsboro, Mali and QC04) and zircon standard 91500 were used in this study (Table 1). The Willsboro garnet was sourced from the Willsboro wollastonite deposit (USA), which has a near end-member andradite ($And_{90}Grs_{10}$) composition and has been suggested as a primary reference material for LA-ICP-MS garnet U—Pb dating (Seman et al., 2017). Based on ID-TIMS analysis, it has a $^{206}Pb/^{238}U$ age of 1022 ± 16 Ma. The relatively high uncertainty might be due to the low U concentrations (1–2 ppm) (Seman et al., 2017). The Mali garnet was sourced from an alluvial deposit in southern Mali. It has an average composition of $And_{52}Grs_{37}$ with higher U concentrations (4.4–7.6 ppm). The ID-TIMS $^{206}Pb/^{238}U$ age is 202.0 ± 1.2 Ma (Seman et al., 2017). The QC04 garnet was collected from the Qicun Fe skarn deposit and has a composition of $And_{90\text{-}98}Grs_{1\text{–}8}$ with the highest U

concentrations (22–118 ppm, Deng et al., 2017) of the three garnet references. Based on LA-ICP-MS U—Pb dating using zircon 91500 as the external standard, it has a concordia lower intercept age of 130 ± 2 Ma and a weighted mean ^{207}Pb-corrected ^{206}Pb/^{238}U age of 130 ± 1 Ma (Deng et al., 2017). The zircon 91500 has been widely used as external standard for zircon U—Pb dating. It is also characterized by high U concentrations (70–100 ppm) and shows an ID-TIMS ^{206}Pb/^{238}U age of 1062.4 ± 0.4 Ma with a concordia age of 1065.4 ± 0.3 Ma (Wiedenbeck et al., 2004).

2.2. Garnet samples from different types of skarn deposits

Garnet samples from different types of skarn deposits, including the Fe, W and Cu—Mo skarn deposits, were tested for U—Pb dating (Table 1). The Jinling Fe skarn deposit, located at the Luxi Block of the eastern North China Craton, is associated with the early Cretaceous (~130 Ma) high-Mg diorite and hosts ~100 million tons of Fe (Lan et al., 2019). At least three generations of grandite garnets are developed in this deposit, which have variable Ca, Al and Fe contents as well as low to high U concentrations (several to tens of ppm) and thus are favorable for studying the garnet U—Pb geochronology.

The Xintianling W skarn deposit is located in the Hunan province of south China. It hosts about 0.33 Mt. of WO_3 and is associated with the late Jurassic (153–163 Ma) Qitianling granite batholith (Yuan et al., 2012). The garnets in this deposit are compositionally Mn-rich grandite garnets and have variable U concentrations (several to tens of ppm). They are commonly intergrown with scheelite, the ages of which can constrain the timing of the W mineralization directly.

The Hongshan Cu—Mo skarn deposit is one of the largest Cu skarn deposits in the Yidun terrane, Yunnan province, southwestern China. It is associated with the late Cretaceous quartz monzonite porphyry (Yang et al., 2016), and the garnet is characterized by the composition of $And_{40-61}Grs_{37-57}$ with high U concentrations (tens of ppm) (Tian et al., 2019).

3. Analytical methods

3.1. SEM and EPMA analyses

Back-scattered electron (BSE) images and chemical compositions of laser-induced particles (analyzed by EDAX) of garnets were acquired using a JSM-7800F SEM (scanning electron microscopy) at the State Key Laboratory of Ore Deposit Geochemistry (SKLODG), Institute of Geochemistry, Chinese Academy of Sciences (IGCAS), Guiyang, China. The analytical conditions were 20 kV accelerating voltage and 10 nA beam current. The crater depths at various spot sizes (24–160 μm) and repetition rates (2, 10 and 20 Hz) for different materials (zircon, glass and garnet) were also measured using a Focused Ion Beam-Scanning Electron Microscope (FIB-SEM, with a z-axis determination limit of 0.1 μm) at the Center for Lunar and Planetary Sciences, IGCAS. The same ablation time of 60 s was used in order to compare the ablation rates of different materials.

Major elements of garnets were analyzed using a JOEL JXA 8230 EPMA (Electron Probe Microanalysis) at the SKLODG. The analytical conditions were 25 kV accelerating voltage and 10 nA beam current. The ZAF program was employed for matrix correction. Mineral standards of almandine (Fe, Mn, Al, Mg and Si), pyrope (Ti and Cr), orthoclase (Na and K), apatite (F), diopside (Ca) and tugtupite (Cl) were used for calibration. The detection limits of the major elements are below 0.01 wt%.

3.2. LA-ICP-MS analysis

Element-distribution mapping of garnets was conducted firstly to see where and how the U, Th and Pb are distributed in the garnets. The mapping was performed at the SKLODG using an Agilent 7700× ICP-MS equipped with a RESOlution S-155 193 nm laser ablation system. A two-volume sample cell is equipped in this system and He (0.35 L/min) and Ar (0.9 L/min) gases mixed in the cell were applied as the carrier gas. The areas of interest were pre-selected based on detailed petrographic observations and then ablated by defining a number of equally spaced lines. The spot size, spacing between individual lines and scanning speed were typically designed to ensure the image resolution with appropriate acquisition time (Ulrich et al., 2009). In this study, lines were ablated using the laser spot size of 15 μm, scanning speed of 10 μm/s, laser fluence of 5 J/cm^2 and repetition rate of 10 Hz. After setting up the appropriate ablation parameters, the analyses were fully automated and driven by the laser software of GeoStar and the mass spectrometer. Processing and imaging of the data were done by the software of Iolite (Paton et al., 2011). The glass standard of NIST610 was used for external calibration while the EPMA determined ^{29}Si was used as internal standard.

Table 2
LA-ICP-MS instrumental setup and the operating conditions.

Laser ablation system	
Laser type	GeoLasPro 193 nm ArF excimer laser
Spot size	24, 32, 44, 60, 90, 120 and 160 μm
Repetition rate	2, 5, 10 and 20 Hz
Fluence	2, 5 and 10 J/cm^2
Sampling mode	Static spot ablation and line scanning
Carrier gas	0.45 L/min He +0.003 L/min N_2
Mass spectrometer	
Instrument	Agilent 7900 ICP-MS
Cooling gas (Ar)	15 L/min
Makeup gas (Ar)	1.0 L/min
RF power	1450 W
Dwell time	6 ms for ^{27}Al, ^{29}Si, ^{43}Ca and ^{57}Fe; 10 ms for ^{202}Hg, ^{204}Pb and ^{208}Pb, ^{232}Th; 20 ms for ^{206}Pb and ^{238}U; 30 ms for ^{207}Pb
ThO^+/Th^+	<0.1%
Th^+/U^+	~100%

LA-ICP-MS U—Pb dating of zircon and garnet was also performed at the above lab using an Agilent 7900 ICP-MS equipped with a GeoLasPro 193 nm ArF excimer laser ablation system. The laser ablation parameters such as spot size, repetition rate and fluence were changed during the experiments to obtain the optimal conditions. The instrumental setup and analytical parameters are summarized in Table 2. A helium flow rate of 0.45 L/min was used to carry the ablated materials to the ICP, with an additional 0.003 L/min N_2 gas added after the ablation cell to enhance the signal sensitivity (Hu et al., 2008). The ICP-MS was tuned to reduce the oxide rate ($ThO^+/Th^+ < 0.1\%$) and doubly charged ion production ($Ca^{++}/Ca^+ < 0.4\%$), maximize the sensitivities of the heavy masses (e.g., U, Th and Pb) and maintain the equal sensitivities of U and Th (^{238}U/^{232}Th ≈ 1) (Günther and Hattendorf, 2005). Each analysis incorporated a background acquisition of approximately 20 s (gas blank) followed by 40 s data acquisition from the sample and 20 s for wash-out. The dwell time of each isotope was adjusted from 6 to 30 ms (Table 2).

3.3. Data reduction

Data reduction including off-line selection and integration of background and analyte signals, time-drift correction and quantitative calibrations was performed using the ICPMSDataCal software (Liu et al., 2010). To ensure that a similar mass bias coefficient k can be obtained (Ulianov et al., 2012), the same length of analyte signals (20–30 s) was chosen for the standards and samples. In order to avoid surface contamination and large particle production, the first 3–5 s analyte signals were abandoned. Large inclusions were screened out during the signal selection and abnormal spikes in the background and analyte signals were filtered.

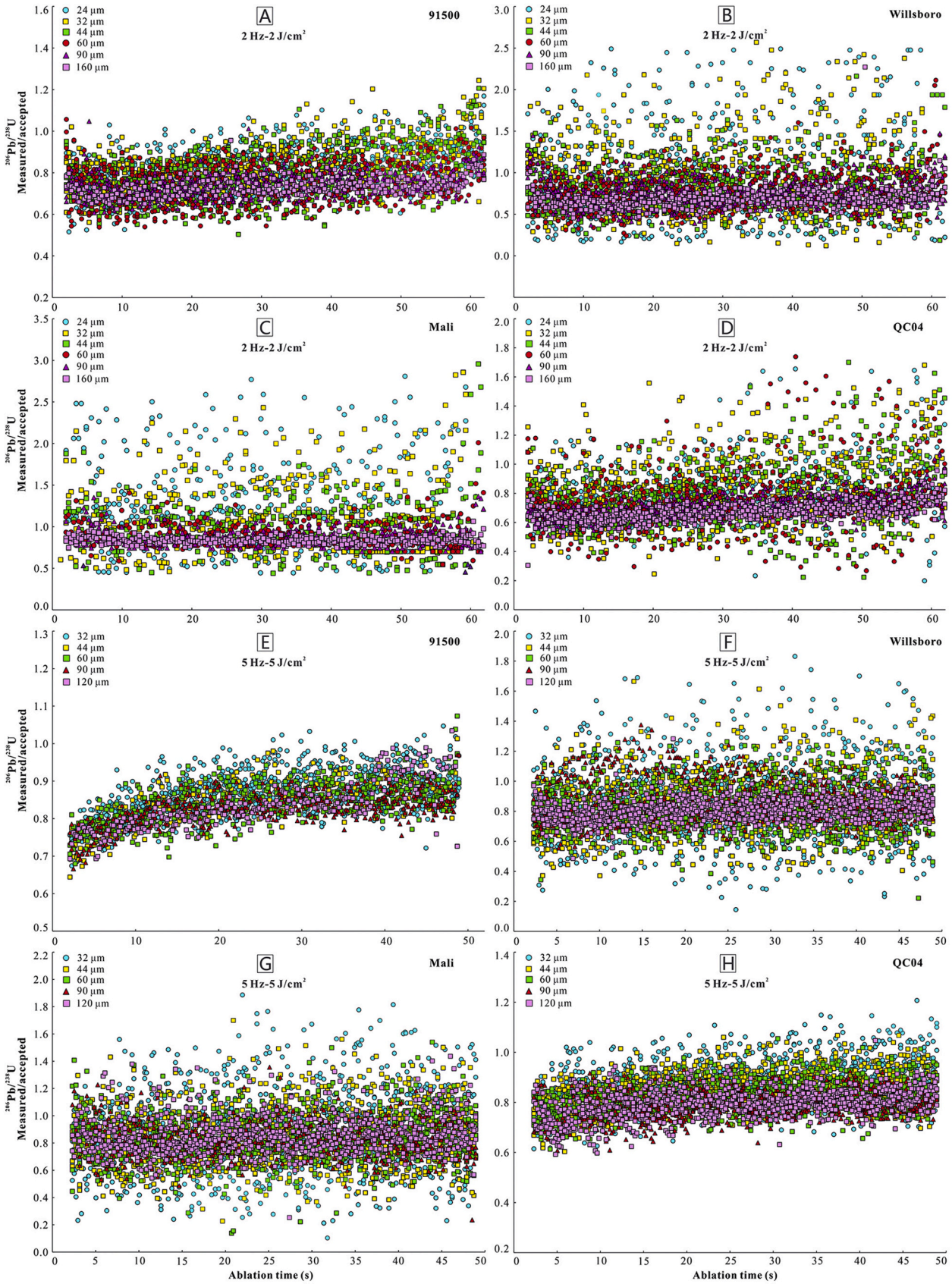

Fig. 1. The ablation behaviors of U and Pb in zircon (91500) and garnets (Willsboro, Mali and QC04) at moderate to low repetition rates (2 and 5 Hz) and fluences (2 and 5 J/cm^2) with a range of spot sizes (24 to 160 μm). The accepted $^{206}Pb/^{238}U$ ratios of 91500, Willsboro and Mali are the weighted mean ratios obtained from ID-TIMS (Wiedenbeck et al., 2004; Seman et al., 2017). Because there is no ID-TIMS data for QC04, the accepted $^{206}Pb/^{238}U$ ratio of QC04 is the theoretical ratio calculated from the terrestrial Pb isotope model (Stacey and Kramers, 1975).

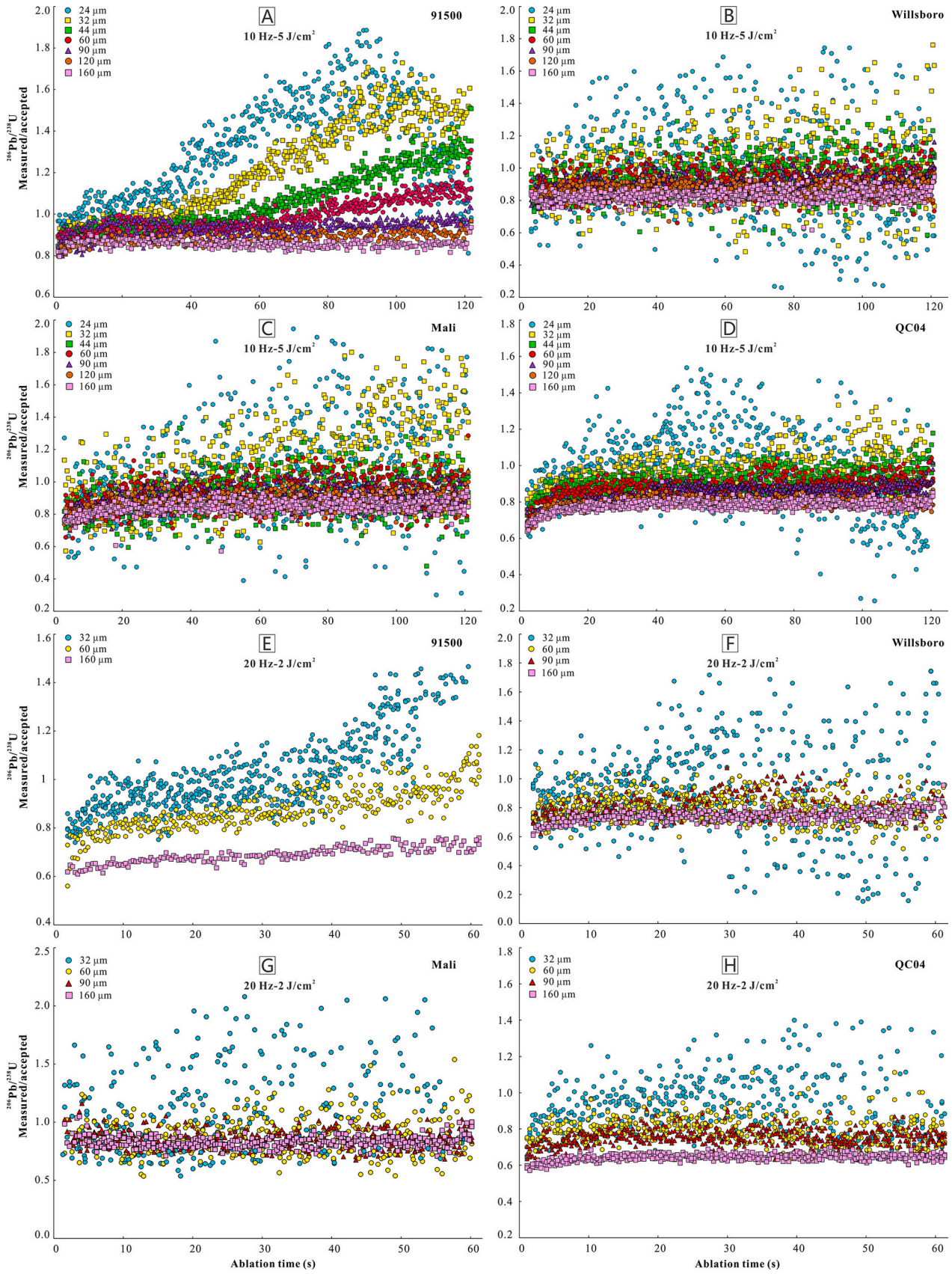

Fig. 2. The ablation behaviors of U and Pb in zircon (91500) and garnets (Willsboro, Mali and QC04) at high repetition rates (10 and 20 Hz) and moderate to low fluences (2 and 5 J/cm^2) with a range of spot sizes (24 to 160 μm). Note that there is a remarkable spot size- and time-dependent U—Pb fractionation in zircon at the high repetition rate (A and E). The accepted $^{206}Pb/^{238}U$ ratios are the same as in Fig. 1.

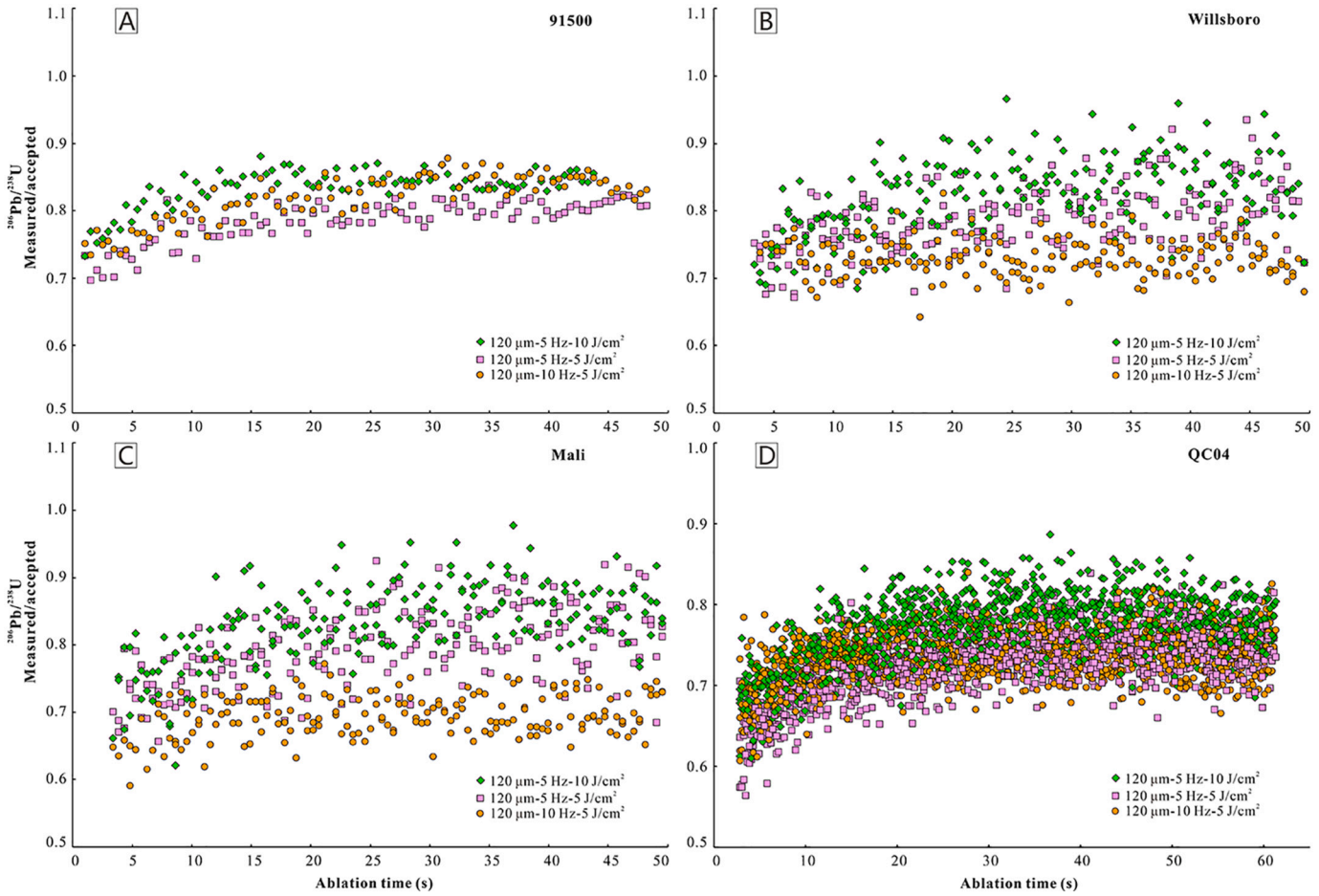

Fig. 3. The ablation behaviors of U and Pb in zircon (91500) and garnets (Willsboro, Mali and QC04) at varied fluences (5 and 10 J/cm^2) and repetition rates (5 and 10 Hz) with a constant spot size of 120 μm. Note that the Pb/U ratios of the high-U samples (91500 and QC04) vary more significantly than the low-U samples with increasing fluence and repetition rate. The accepted $^{206}Pb/^{238}U$ ratios are the same as in Fig. 1.

3.4. Common Pb correction and age calibration

For a U—Pb age calibration, common Pb should be typically considered for the accessory minerals due to the variable amounts of common Pb (Chew et al., 2014). Many approaches have been used for common Pb correction (Williams, 1998; Gregory et al., 2007; Chew et al., 2014; El Korh, 2014), which commonly require an estimation of initial common Pb ratios using the terrestrial Pb isotope model (Stacey and Kramers, 1975). The approaches assume that no unsupported radiogenic Pb was inherited from a precursor mineral (Romer and Siegesmund, 2003; Gregory et al., 2007; El Korh, 2014). The proportion of common Pb can be simply assessed through the following way (Gregory et al., 2007):

$$f_{206} = {}^{206}Pb_c/{}^{206}Pb_{total} = \left({}^{207}Pb/{}^{206}Pb_m - {}^{207}Pb/{}^{206}Pb^*\right)/\left({}^{207}Pb/{}^{206}Pb_c - {}^{207}Pb/{}^{206}Pb^*\right)$$

where f_{206} is the amount of common ^{206}Pb expressed as a fraction of the total ^{206}Pb, $^{207}Pb/^{206}Pb_m$ is the measured ratio, $^{207}Pb/^{206}Pb^*$ is the expected radiogenic ratio for the inferred age and $^{207}Pb/^{206}Pb_c$ is the common Pb composition. The f_{206} could vary between 0 and 1. The f_{206} values of the reference materials (91500, Willsboro, Mali and QC04) used in this study are lower than 0.01, corroborating that they contain very low common Pb (Wiedenbeck et al., 2004; Deng et al., 2017; Seman et al., 2017). Two widely-used methods were adopted for age calibration: (1) the uncorrected data were plotted on the Tera-Wasserburg diagram ($^{207}Pb/^{206}Pb$-$^{238}U/^{206}Pb$) (Tera and Wasserburg, 1972), where a linear regression through the plots yields a lower intercept age that represents the garnet age; (2) the ^{207}Pb-based correction method (Williams, 1998; Aleinikoff et al., 2002), which can give rise to an individual $^{206}Pb/^{238}U$ age for each analysis by assuming an initial $^{207}Pb/^{206}Pb$. The initial $^{207}Pb/^{206}Pb$ was estimated by the Tera-Wasserburg regression line that determines the initial $^{207}Pb/^{206}Pb$ ratio on the *y*-axis intercept (El Korh, 2014). Concordia diagram and weighted mean $^{206}Pb/^{238}U$ age calculation were processed using the Isoplot software (Ludwig, 2003).

4. Results and discussion

4.1. U—Pb fractionation in zircon and garnet during laser ablation

Due to the large difference in matrix composition, it is inferred that U and Pb behave differently between the zircon and garnet during laser ablation. It has been recognized that laser-induced fractionation depends on ablation parameters such as spot size, repetition rate and laser fluence (Ulianov et al., 2012), the effects of which were thus investigated in detail.

4.1.1. Effects of spot size, repetition rate and laser fluence

The effects of spot size, repetition rate and laser fluence were tested using a range of spot sizes (24, 32, 44, 60, 90, 120 and 160 μm) to ablate the zircon standard 91500 and the garnet reference materials (Willsboro, Mali and QC04) at low to high fluences (2, 5 and 10 J/cm^2) and repetition rates (2, 5, 10 and 20 Hz). The results show that at the moderate to low repetition rates (2 and 5 Hz) no significant U—Pb fractionation occurs in both the zircon and garnet samples with varied

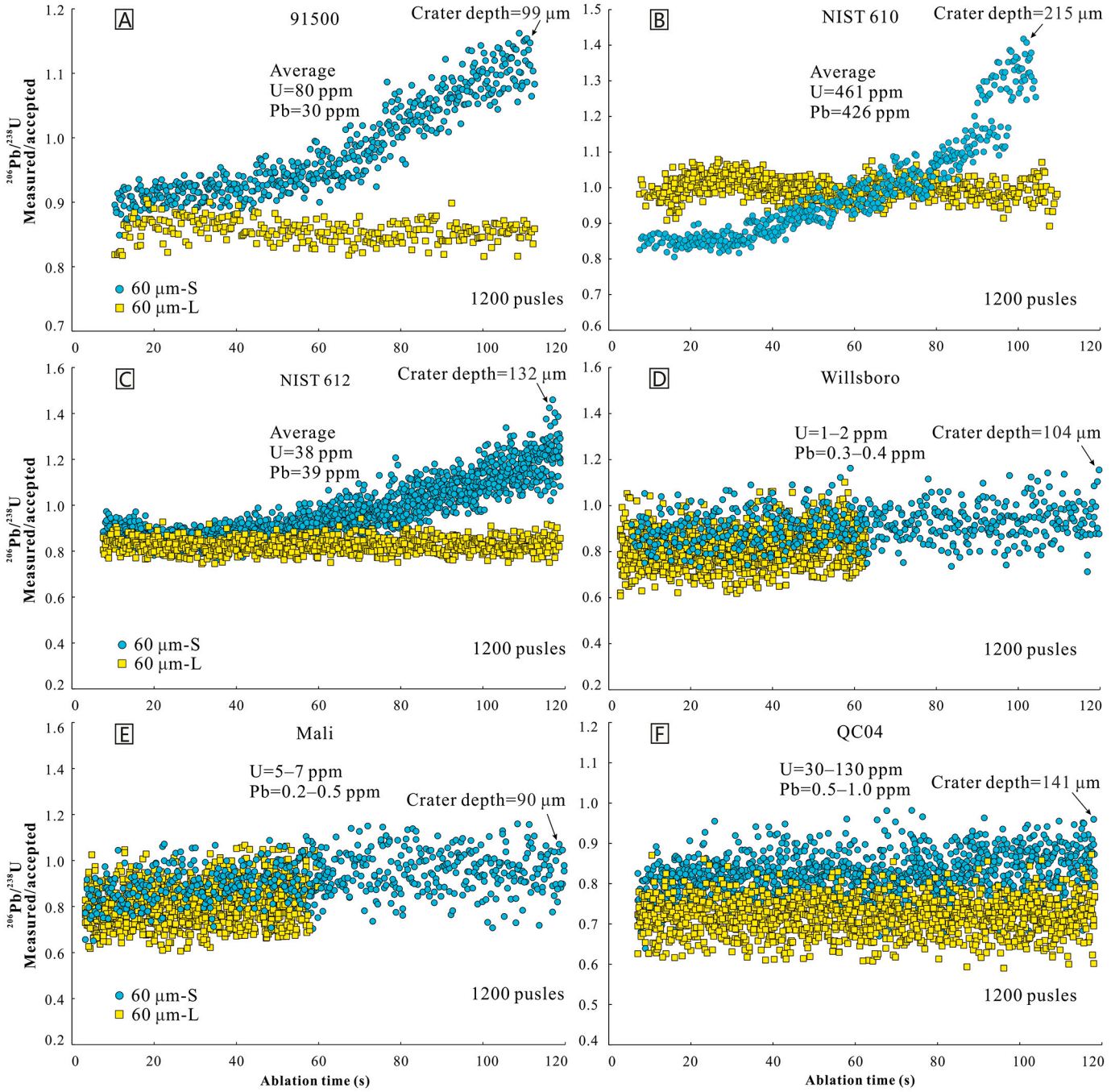

Fig. 4. Comparison of U—Pb fractionation between spot analysis and line scanning for zircon (91500), glasses (NIST 610 and 612) and garnets (Willsboro, Mali and QC04), illustrating that line scanning can effectively minimize or eliminate the U—Pb fractionation. Spot size of 60 μm, repetition rate of 10 Hz and fluence of 5 J/cm^2 were used for both the spot analysis and line scanning. Crater depths in spot analysis are marked to show that different materials have different ablation rates, which could exert effects on depth-dependent U—Pb fractionation. S = spot analysis; L = line scanning. The accepted $^{206}Pb/^{238}U$ ratios are the same as in Fig. 1.

spot sizes (24 to 160 μm) and fluences (2 and 5 J/cm^2) (Fig. 1), although a slight time-dependent (also called downhole/depth-dependent) U—Pb fractionation occurs at 5 Hz in the zircon 91500 (Fig. 1E). There are larger fluctuations of Pb/U ratios at the smaller spot sizes (e.g., 24 and 32 μm), which are likely due to the lower contents of U and Pb ablated. By contrast, at the higher repetition rates (10 and 20 Hz), a significant time-dependent U—Pb fractionation occurs in zircon but not in garnets (Fig. 2). The time-dependent U—Pb fractionation becomes enhanced as the spot size decreases, which can be minimized by large spot sizes (e.g., ≥90 μm) (Fig. 2A and E). In addition, the Pb/U ratios of the high-U samples (91500 and QC04) increase with decreasing spot size (Fig. 2A, D, E and H). This almost does not occur in the low-U samples (Willsboro and Mali) (Fig. 2B, C, F and G).

The effects of laser fluence and repetition rate were further tested at varied fluences (5 and 10 J/cm^2) and repetition rates (5 and 10 Hz) with a constant spot size of 120 μm (Fig. 3). It shows that enhanced laser fluence has little effect on the time-dependent U—Pb fractionation, but leads to a slight increase of Pb/U ratio for the high-U samples (91500 and QC04). Elevating repetition rate leads to the Pb/U ratio increasing slightly in the high-U samples but decreasing in the low-U samples.

The above results indicate that large spot sizes (e.g., ≥90 μm) and low repetition rates (e.g., 2–5 Hz) are favorable for minimizing the

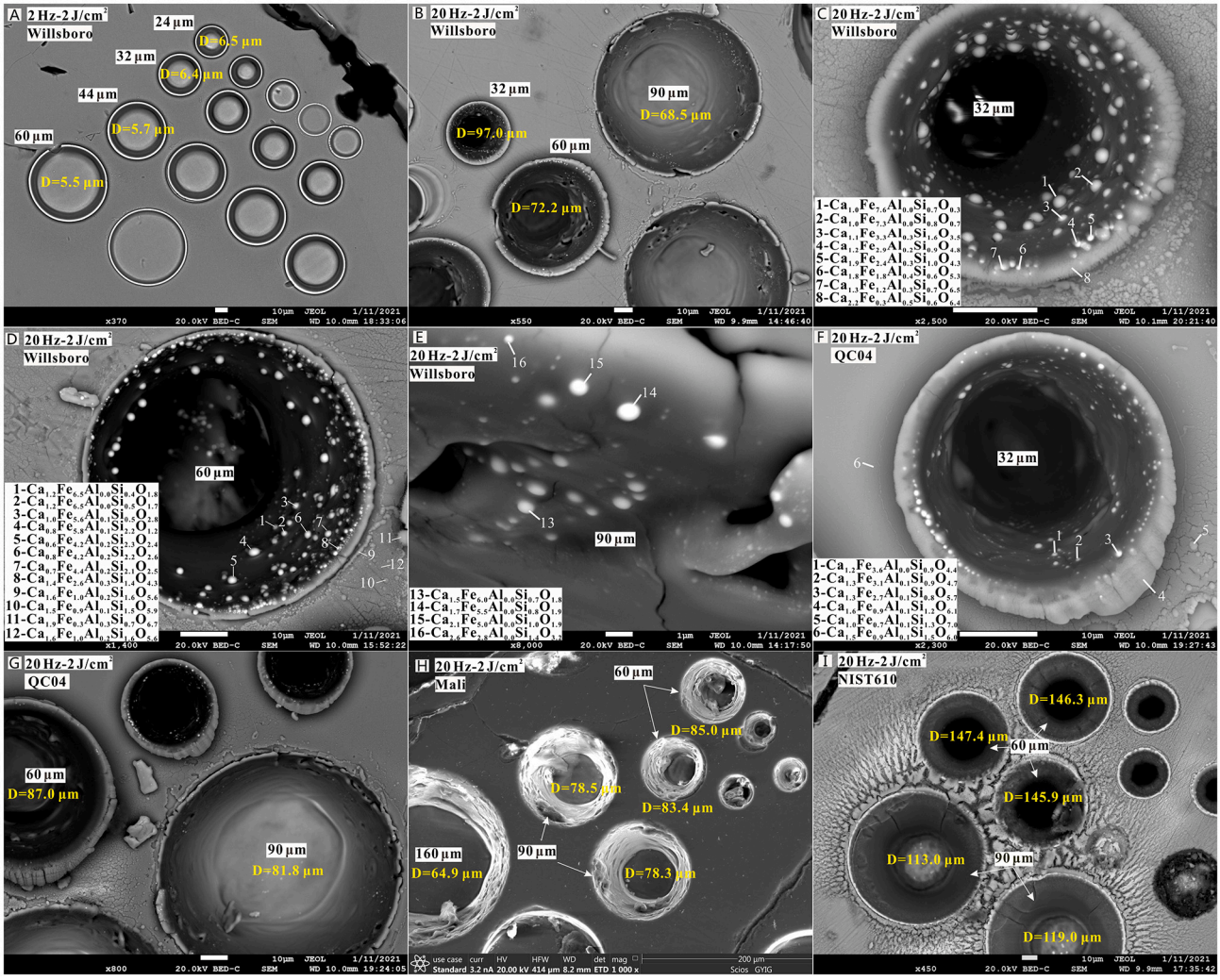

Fig. 5. The distributions and compositions of laser-produced particles and the crater depths at various ablation parameters. The micrographs were obtained from BSE (Back-scattered Electron) imaging and the compositions of the particles were analyzed by EDAX (Energy Dispersive X-ray Analysis). Note that the crater depths of different materials (Willsboro, Mali and QC04 and NIST 610) show a decrease with decreasing repetition rate or increasing spot size. D = crater depth.

U—Pb fractionation in zircon and garnet. The effects of fluence on U—Pb fractionation are more significant in high-U samples than in low-U samples.

4.1.2. Line scanning vs. spot analysis

Line scanning ablation has been proved to be effective in minimizing the time-dependent U—Pb fractionation and thus been widely used in non-matrix-matched U—Pb dating of accessary minerals such as apatite (Chew et al., 2011), allanite (Darling et al., 2012) and titanite (Storey et al., 2006; Li et al., 2010). In this study, the line scanning ablation was tested on zircon and garnet at the spot size of 60 μm, repetition rate of 10 Hz, fluence of 5 J/cm^2 and scanning speed of 3 μm/s. To compare the results, spot analysis was carried out at the same ablation parameters. Glass standards of NIST 610 and 612 were also analyzed for comparison. The results show that besides the commonly observed phenomenon that time-dependent U—Pb fractionation in zircon and glass can be eliminated by the line scanning, it is notable that almost no time-dependent U—Pb fractionation occurs in garnets under both the line scanning and spot analysis modes (Fig. 4). It is also notable that, compared with the low-U samples (e.g., Willsboro and Mali), the Pb/U ratios of the high-U samples (e.g., 91500, NIST 610 and QC04) show enhanced difference between the line scanning and spot analysis.

4.1.3. Types and mechanisms of U—Pb fractionation

Previous studies showed that U—Pb fractionation during LA-ICP-MS analysis can be resulted from laser-induced, transport-induced and ICP-induced processes. The laser-induced fractionation is associated with the thermal decomposition and the formation of non-stoichiometric aerosol particles during the laser-sample interaction, whereas the transport-induced fractionation refers to the selective particle deposition during the transportation, and the ICP-induced fractionation occurs whenever transported particles are not completely ionized within the ICP (Fryer et al., 1995; Outridge et al., 1997; Horn et al., 2000; Guillong et al., 2003; Koch et al., 2004; Kuhn et al., 2004; Garcia et al., 2007; Machida et al., 2015; Fietzke and Frische, 2016). Considering that all the samples in this study were analyzed under the same ICP-MS conditions and the working conditions were optimized, the ICP-induced fractionation is not discussed in this study. The laser- and transport-induced fractionation can be constrained based on detailed investigations on the distributions and compositions of the laser-produced particles (Guillong et al., 2003; Košler et al., 2005). Under the SEM imaging, the particles of garnets were deposited on the floors, walls or the surfaces around the craters (Fig. 5). They are mostly spherical with sizes varying between nanometer and micrometer (<3 μm). There are three important trends identified: (1) the amounts of particles produced at the low repetition rate (e.g., 2 Hz) are much less than those produced at the high repetition

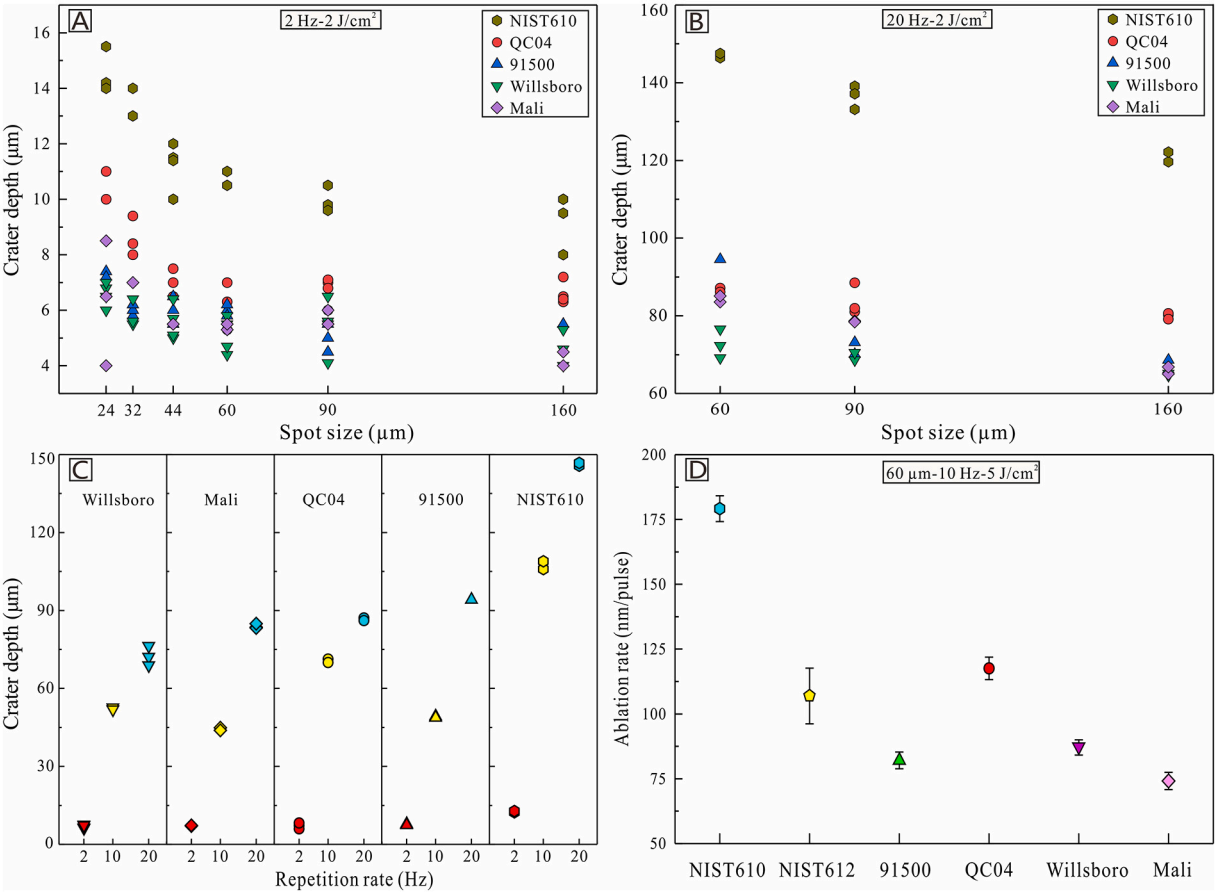

Fig. 6. The crater depths of different materials (zircon, glass and garnet) at various spot sizes and repetition rates (A–C) and the comparison of ablation rates among them (D).

rate (e.g., 20 Hz) (Fig. 5A and B), (2) the particles deposited on the crater wall become fewer as the spot size increases (Fig. 5B) and (3) the sizes of the particles deposited on the crater wall generally decrease with increasing spot size (Fig. 5C–E). These trends indicate that both the low repetition rate and large spot size facilitate the ablated materials to be transported to the ICP. In addition, it is also found that the crater depths of the analyzed materials (zircon, glass and garnet) show a decrease with decreasing repetition rate or increasing spot size (Fig. 5A, B, G–I and 6), indicating that both the low repetition rate and large spot size can slow down the ablation rate. This is meaningful for mitigating the downhole-dependent U—Pb fractionation. Therefore, the above results suggest that laser- and transport-induced U—Pb fractionation commonly occur in the studied materials during laser ablation, but can be minimized by low repetition rate and large spot size (Figs. 1 and 2). Notably, different materials have different ablation rates (Fig. 6D), which could lead to contrasted depth-dependent U—Pb fractionation (Fig. 4). It is thus necessary to evaluate the effects of ablation rate during LA-ICP-MS U—Pb dating .

It is noted that the chemical compositions (analyzed by EDAX in the SEM) of the particles from the garnets show a spatial variation. For example, the Fe contents of the particles (Willsboro and QC04) decrease gradually from the inner wall to the rim and then to the distal surface of the crater while the Si + O contents increase (Fig. 5C–F). The spatial variation of particle compositions has also been observed in the other materials such as zircon and NIST glasses (Košler et al., 2005), which were considered to be resulted from thermal decomposition and be responsible for the downhole-dependent U—Pb fractionation. For the zircon, it was proposed that ZrO_2 and SiO_2 particles are generated during laser ablation, of which the ZrO_2 particles are favorably deposited on the inner wall or the surface around the crater. Because U is preferentially partitioned into the ZrO_2 particles while Pb not, the increasing deposition of ZrO_2 particles leads to the increase of the Pb/U ratio as the crater depth increases (Košler et al., 2005). For the garnet, a similar thermal decomposition might occur, but leads to weak U—Pb fractionation due to the different mechanisms of U incorporated into the particles. As mentioned before, the garnets in this study were decomposed into Fe-rich and Si + O-rich particles with a spatial distribution, in which the Ca contents keep relatively stable (Fig. 5C–F). Because U incorporation into grandite garnets is mainly controlled by the coupled substitution of $[Ca^{2+}]^{VII}_{-1}[REE^{3+},U^{4+}]^{VII}_{+1}[Si^{4+}]^{IV}_{-1}[Fe^{3+},Al^{3+}]^{IV}_{+1}$ (Gaspar et al., 2008; Deng et al., 2017), especially the U substitutes Ca due to their similar ionic radii (Smith et al., 2004; Gaspar et al., 2008), the constant Ca contents make the U to be unfractionated as the ablation proceeds. This thus leads to the little depth-dependent U—Pb fractionation in the garnets (Figs. 1, 2 and 4).

The above mechanisms cannot well explain the $^{206}Pb/^{238}U$ ratios of the high-U samples (e.g., 91500, QC04 and NIST 610) increasing with elevated fluence (e.g., from 5 to 10 J/cm^2) or with decreasing spot size at the high repetition rate (e.g., ≥10 Hz) (Figs. 2 and 3). It has been proposed that during laser ablation U and Pb are refractory and volatile elements, respectively, which can be fractionated from each other due to their different vaporization and transportation properties, leading to the Pb/U ratio changing with crater depth or spot size (Eggins et al., 1998; Mank and Mason, 1999; Horn et al., 2000). Based on this consideration, in combination with higher fluence and repetition rate leading to higher ablation temperature (Eggins et al., 1998; Horn et al., 2000), it is inferred that the fractionation between U and Pb is enhanced at the high fluence and repetition rate conditions (Outridge et al., 1997; Horn et al.,

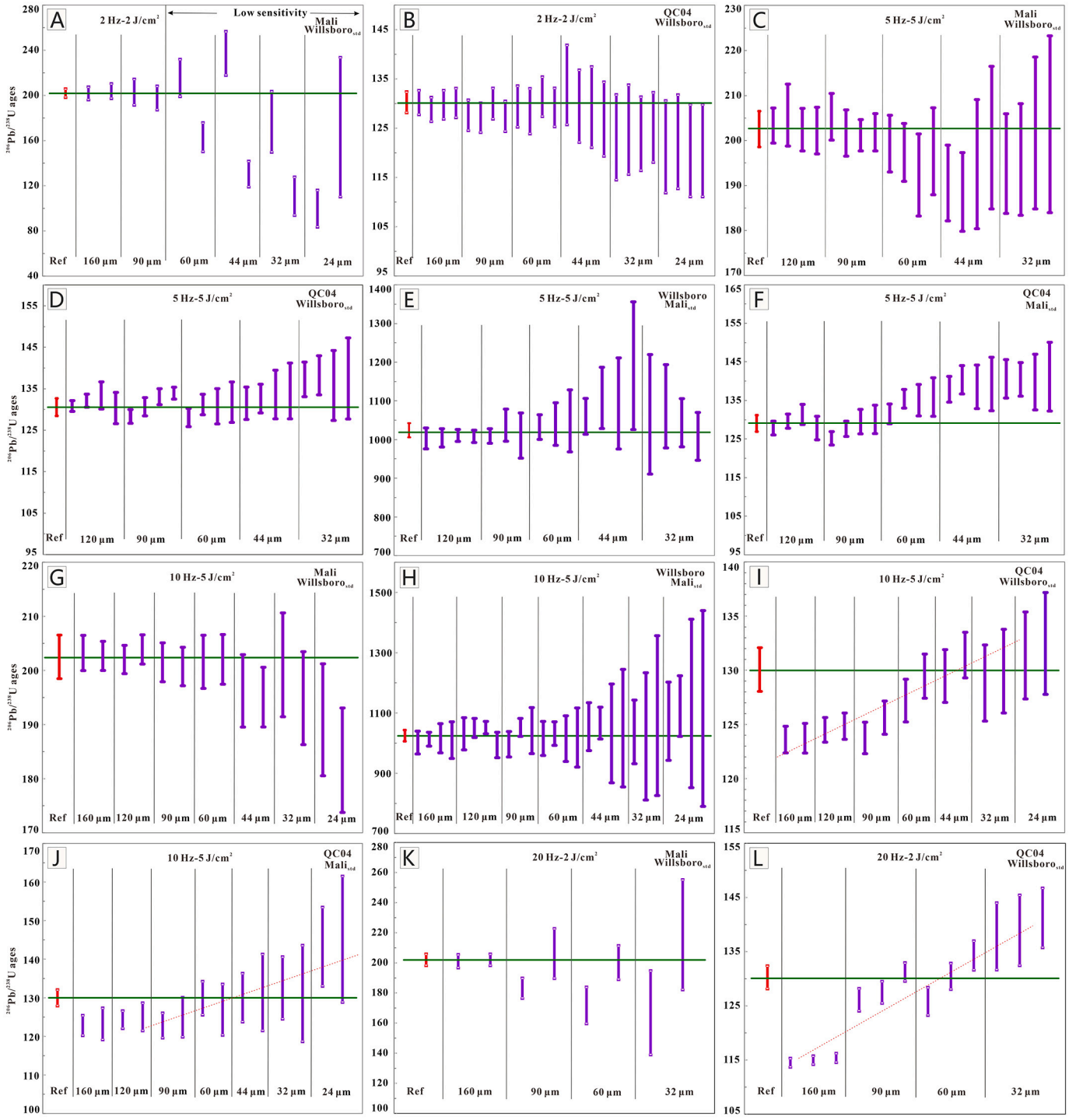

Fig. 7. The ^{207}Pb-corrected $^{206}Pb/^{238}U$ ages of the garnets (Willsboro, Mali and QC04) obtained from various spot sizes, repetition rates and fluences under the matrix-matched condition. The Willsboro and Mali were used as external standard, respectively.

2000). The high U concentrations in the high-U samples reinforce the above fractionation.

Another remarkable phenomenon is that most of the measured $^{206}Pb/^{238}U$ ratios by LA-ICP-MS are lower than the accepted values (measured by ID-TIMS or theoretical ratio) (Figs. 1, 2 and 3), especially for the high-U samples (91500 and QC04) at the large spot sizes (e.g., ≥120 μm) coupled with high repetition rate (e.g., ≥10 Hz). The difference in Pb/U ratio between LA-ICP-MS and ID-TIMS analyses has been typically observed in zircon, which could lead to the age deviation during LA-ICP-MS U—Pb dating (Allen and Campbell, 2012; Steely et al., 2014; Marillo-Sialer et al., 2016; Sliwinski et al., 2017). Although the mechanism is still controversial, alpha dose (radiation damage) has been considered to play a role. Allen and Campbell (2012) considered that Pb escapes more readily than U around the margin of the ablation hole in radiation damaged sample, leading to the increase of $^{206}Pb/^{238}U$ with increasing radiation damage. Other studies suggested that alpha dose can lead to the faster laser ablation rate, which might exert the effect on U—Pb fractionation (Steely et al., 2014; Marillo-Sialer et al., 2016; Sliwinski et al., 2017). In this study, the high-U garnet (QC04) show much higher ablation rate than those of the low-U garnets (Willsboro and

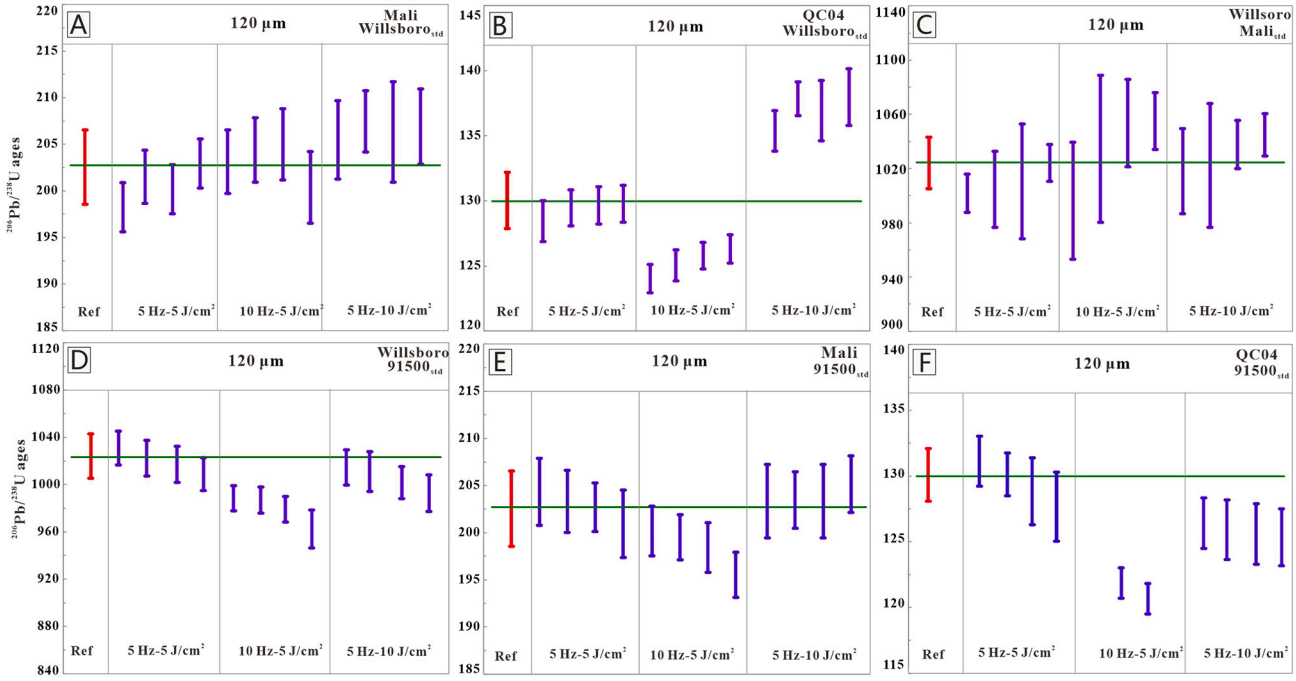

Fig. 8. The ^{207}Pb-corrected $^{206}Pb/^{238}U$ ages of the garnets (Willsboro, Mali and QC04) obtained from various repetition rates (5 and 10 Hz) and fluences (5 and 10 J/cm^2) at a constant spot size of 120 μm under the matrix-matched (A–C) and non-matrix-matched (D—F) conditions, illustrating the effects of repetition rate and fluence on U—Pb age.

Mali) (Fig. 6D), in combination with its enhanced derivation in Pb/U ratio from the accepted value (Fig. 2D and H), indicating that stronger effects of alpha dose likely occurred in the high-U garnet. The mechanisms of alpha dose on U—Pb fractionation in garnet should be further tested based on detailed comparison between the LA-ICP-MS and the ID-TIMS analyses.

In summary, there are at least three types of U—Pb fractionation identified in the studied samples. The first type is the time-dependent or downhole-dependent (significant in zircon but not in garnets), which has been well known. The second type is related to the intrinsic properties of U (more refractory) and Pb (more volatile), which can be affected by the laser fluence or repetition rate. The third type is the alpha dose-dependent, which is associated with the crystal lattice damage and thus the U and/or Th concentrations. These types of U—Pb fractionation typically suggest that low-U and high-U samples should be treated differently during U—Pb dating due to their different U—Pb fractionation coefficients.

4.2. U—Pb ages at matrix-matched and non-matrix-matched conditions

It is almost impossible to find a perfectly matrix-matched external standard for garnet U—Pb dating due to the variable compositions of natural garnet. Nonetheless, in this study, using garnet as external standard is considered as matrix-matched while using other materials (e.g., zircon) is considered as non-matrix-matched. Corresponding to the experiments for U—Pb fractionation, the age determinations of grandite garnets (Willsboro, Mali and QC04) were also conducted at various spot sizes (24, 32, 44, 60, 90, 120 and 160 μm), repetition rates (2, 5, 10 and 20 Hz) and fluences (2, 5 and 10 J/cm^2) using Willsboro, Mali and 91500 as external standard, respectively. The U—Pb isotopic data are listed in Supplementary Data.

4.2.1. Ages at matrix-matched

All the analyzed garnets can be accurately dated at the moderate to low repetition rates (2 and 5 Hz) and fluences (2 and 5 J/cm^2) coupled with a large spot size (e.g., ≥90 μm) when using either Willsboro or Mali as the external standard (Fig. 7A–F). As the spot size becomes smaller (≤60 μm), the ages of the Willsboro, Mali and QC04 become continuously younger or older with larger uncertainties. At the higher repetition rate of 10 Hz (coupled with fluence of 5 J/cm^2), the Willsboro and Mali can also be accurately dated at the spot sizes larger than 60 μm (Fig. 7G and H), but the ages become either younger or older as the spot size deceases (e.g., ≤44 μm). For the high-U garnet (QC04), the age shows a continuous increase from the large to the smaller spot sizes (160 to 24 μm) (Fig. 7I and J). The acceptable age (within 1% deviation from the recommended age) occurs at the spot sizes of 60 to 32 μm with large uncertainties. At more extreme conditions (20 Hz coupled with 2 J/cm^2), very large spot sizes (e.g., 160 μm) are required to get the accurate age for the low-U garnet (Mali) (Fig. 7K). Smaller spot sizes (e.g., ≤90 μm) lead to serious scatter of the age. For the high-U garnet (QC04), the age shows a continuous increase from the large to the smaller spot sizes (160 to 24 μm) (Fig. 7L), similar to the trend obtained at the repetition rate of 10 Hz (Fig. 7I). The acceptable age can be obtained at the spot sizes varying between 90 and 60 μm, but large uncertainties occur.

The effects of repetition rate and fluence on U—Pb age were further evaluated by setting a constant spot size of 120 μm with varied repetition rates (5 and 10 Hz) and fluences (5 and 10 J/cm^2). The results show that the ages of the Willsboro and Mali can be accurately obtained at the lower repetition rate and fluence (5 Hz + 5 J/cm^2), but increase 2–5% to the higher repetition rate (10 Hz + 5 J/cm^2) or higher fluence (5 Hz + 10 J/cm^2) (Fig. 8A–C).

4.2.2. Ages at non-matrix-matched

When using 91500 as the external standard, the Willsboro can be accurately dated at the low repetition rate (2 Hz) and fluence (2 J/cm^2) coupled with a moderate-large spot size (e.g., 60–90 μm) (Fig. 9A). Under the same condition, the Mali and QC04 cannot be well dated (Fig. 9B and C). At the moderate repetition rate (5 Hz) and fluence (5 J/cm^2), the low-U garnets (Willsboro and Mali) can be accurately dated using large spot sizes (e.g., ≥120 μm) (Fig. 9D and E). The ages will become either younger or older than their recommended ages (2–5% derivation) with larger uncertainties as the spot size deceases (e.g., <90

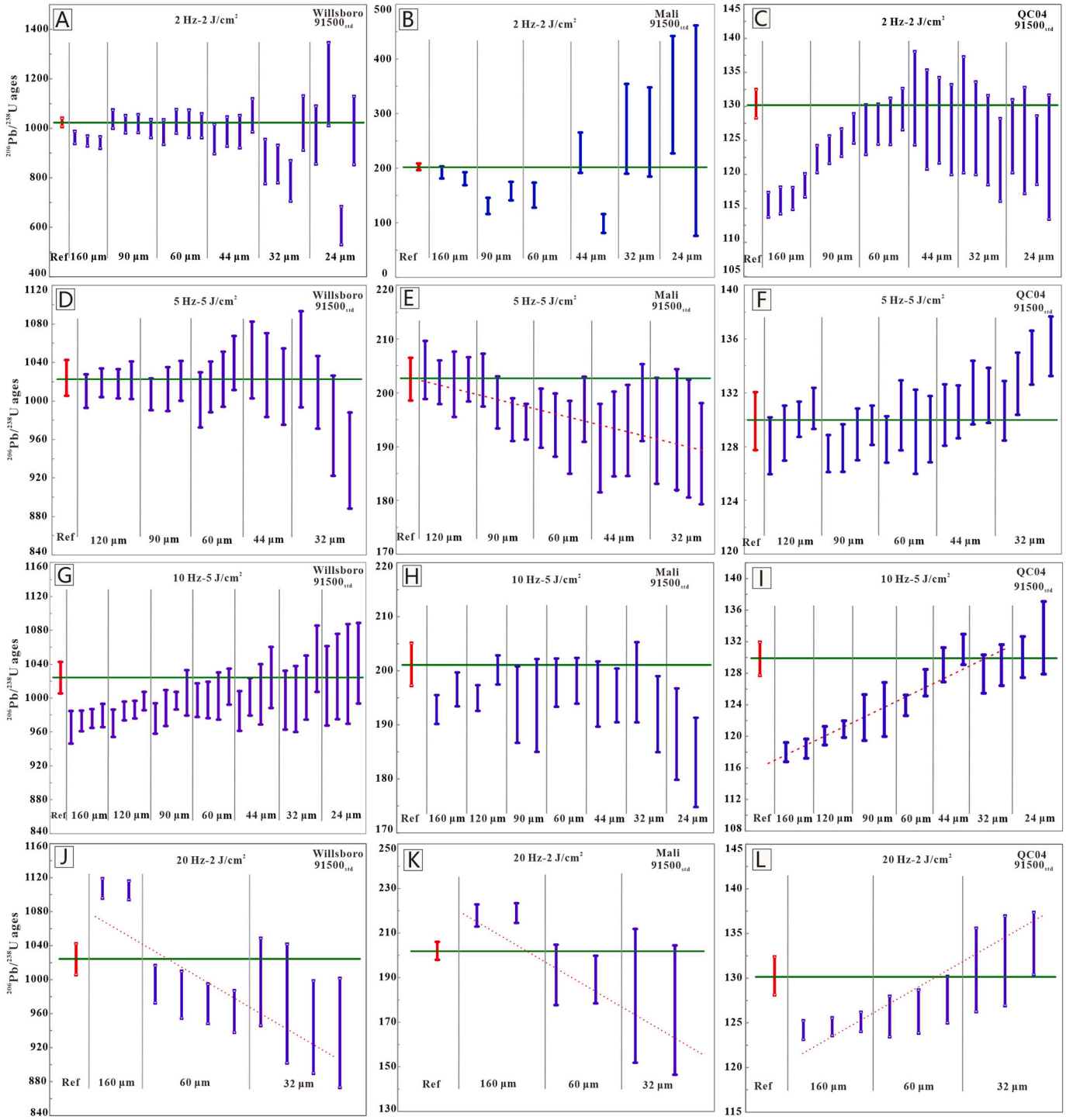

Fig. 9. The ^{207}Pb-corrected ^{206}Pb/^{238}U ages of the garnets (Willsboro, Mali and QC04) obtained from various spot sizes, repetition rates and fluences under the non-matrix-matched condition. Zircon 91500 was used as external standard.

μm). The high-U garnet (QC04) shows the age increasing continuously from the large to the smaller spot sizes (Fig. 9F). The acceptable age (within 1% deviation from the recommended age) can be obtained at the spot size of 60 μm. At the higher repetition rate of 10 Hz (coupled with 5 J/cm^2), it is difficult to obtain the accurate ages for all the garnets (Fig. 9G–I), although acceptable ages for Willsboro and QC04 can be achieved at the relatively small spot sizes (e.g., 24–44 μm). The ages of Mali are always younger than its recommended value at all the used spot sizes. Under more extreme conditions (20 Hz + 2 J/cm^2), none of the garnets can be accurately dated. The ages either show serious deviations (2–10%) or have large uncertainties (Fig. 9J–L).

The effects of repetition rate and fluence on U—Pb age were also tested at a constant spot size of 120 μm with varied repetition rates (5 and 10 Hz) and fluences (5 and 10 J/cm^2). The results show that the ages of all the garnets can be best obtained at the lower repetition rate and fluence (5 Hz + 5 J/cm^2) (Fig. 8D–F).

4.2.3. *Ages from line scanning*

Line scanning is effective to eliminate the U—Pb fractionation in different materials (Fig. 4), which is thus hoped to work well for the

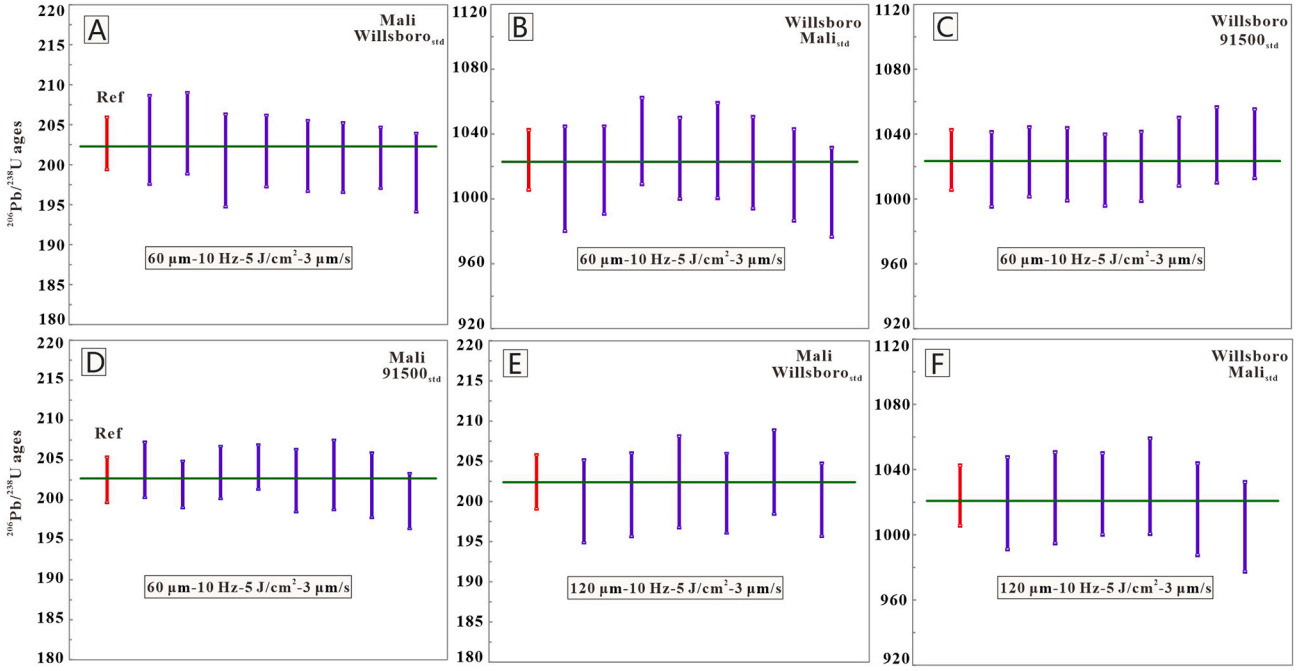

Fig. 10. The ^{207}Pb-corrected ^{206}Pb/^{238}U ages of the garnets (Willsboro and Mali) obtained from line scanning under both the matrix-matched and non-matrix-matched conditions.

garnet U—Pb dating. This is confirmed by the resultant ages. At a constant spot size of 60 μm, repetition rate of 10 Hz, fluence of 5 J/cm^2, and scanning speed of 3 μm/s, the U—Pb ages of the Willsboro and Mali are consistent with their reference ages no matter using garnet or zircon as the external standard (Fig. 10A–D). Increasing spot size (from 60 to 120 μm) results in minor effect on the U—Pb ages (Fig. 10E and F).

4.3. Optimal conditions for garnet U—Pb dating

Based on the above results, it is clear that U—Pb fractionation and matrix effects during laser ablation can be well minimized or eliminated by line scanning. The U—Pb ages of different grandite garnets can be accurately obtained at broad ablation parameters under both the matrix-matched and non-matrix-matched conditions. It is thus strongly suggested to use the line scanning for garnet U—Pb dating if possible (e.g., the garnet is large enough without complex zoning). However, natural garnets commonly have multiple generations of growth or are small in size, which require spot analysis. The ablation parameters under spot analysis thus need to be optimized due to the various U—Pb fractionation under different conditions.

4.3.1. For matrix-matched

Both the experiments on U—Pb fractionation and calibrations on U—Pb age show that moderate to low repetition rates (2–5 Hz) and fluences (2–5 J/cm^2) coupled with a large spot size (≥90 μm) are favored by all the grandite garnets under the matrix-matched condition. However, because the U—Pb fractionation shows some difference between the low-U (e.g., Willsboro and Mali, 1–7 ppm U) and high-U garnets (e.g., QC04, 30–130 ppm U), the garnets having different U concentrations are best treated differently. For the low-U garnets, besides the above ablation parameters, moderate to large spot sizes (e.g., ≥60 μm) coupled with a high repetition rate and moderate fluence (e.g., 10 Hz + 5 J/cm^2) can also be applied. For the high-U garnets, if using the same repetition rate and fluence (10 Hz + 5 J/cm^2), smaller spot sizes (e.g., 32–44 μm) are required. Too low or high repetition rates (e.g., <2 Hz and > 10 Hz) and fluences (e.g., <2 J/cm^2 and > 10 J/cm^2) are not favored, because elevated U—Pb fractionation or large uncertainties will occur under these conditions.

The different ablation parameters required for low-U and high-U garnets suggests that U concentration-matched external standards are important for precise U—Pb dating. Because the available primary reference material (Willsboro) is low in U concentrations (1–2 ppm) (Seman et al., 2017), it is necessary to develop moderate- to high-U garnet standards.

4.3.2. For non-matrix-matched

Previous studies used various spot sizes (e.g., 44–257 μm), repetition rates (5–15 Hz) and fluences (1.5–6 J/cm^2) to ablate garnets when using the non-matrix-matched materials such as zircon standards of 91500 and GJ-1 or the glass standards of NIST 614 and 612 as the external standards (e.g., Wafforn et al., 2018; Burisch et al., 2019; Yan et al., 2020; Bineli Betsi et al., 2020). This study shows that the ablation parameters required to accurately date the garnets under non-matrix-matched condition are more restricted than those under matrix-matched conditions. All the garnets (including low-U and high-U garnets) can be accurately dated at the conditions of large spot sizes (e.g., ≥120 μm) coupled with a moderate repetition rate (e.g., 5 Hz) and fluence (e.g., 5 J/cm^2) when using zircon 91500 as the external standard. Smaller spot sizes (e.g., 32–44 μm) coupled with a high repetition rate (e.g., 10 Hz) and moderate fluence (e.g., 5 J/cm^2) can be applied to some garnets (e.g., Willsboro and QC04). Too high or low repetition rates (e.g., ≤2 Hz and ≥ 10 Hz) and fluences (e.g., ≤2 J/cm^2 and ≥ 10 J/cm^2) are also not favored.

4.3.3. Mass bias correction coefficient k

Mass bias correction coefficient k is associated with the isotope concentration ratio and intensity ratio, which can provide useful information to evaluate the ablation behaviors of U and Pb through time and the matrix effects that occur between different materials (Ulianov et al., 2012; Burn et al., 2017). The coefficient k for ^{238}U and ^{206}Pb is defined as follows (Ulianov et al., 2012):

$$k = \left(\frac{C_{std}^{206Pb}}{C_{std}^{238U}}\right) \Big/ \left(\frac{I_{std}^{206Pb}}{I_{std}^{238U}}\right) \text{ or } = \left(\frac{C_{std}^{206Pb}}{C_{std}^{238U}}\right) \times \left(\frac{I_{std}^{238U}}{I_{std}^{206Pb}}\right)$$

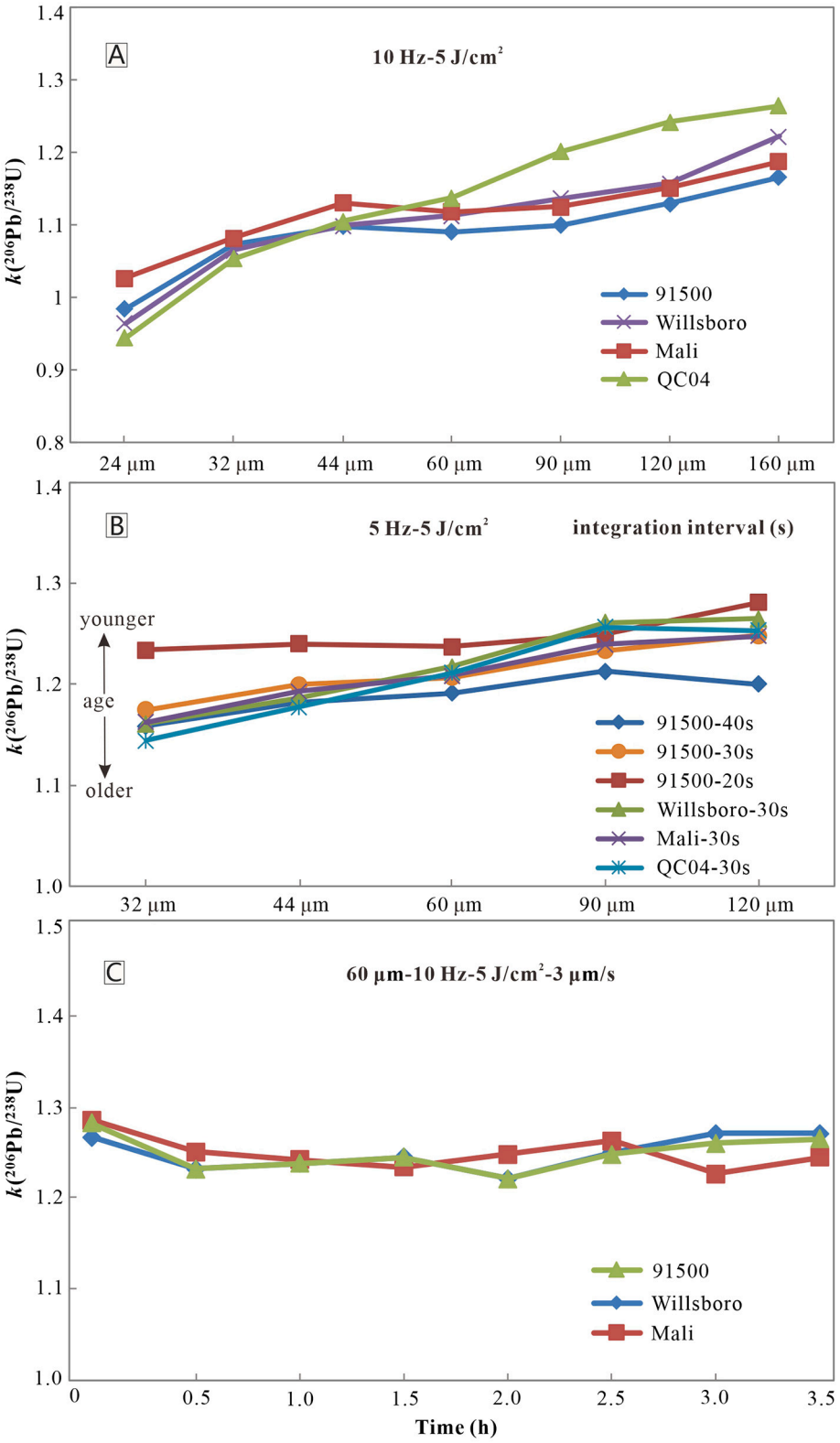

Fig. 11. Comparison of mass bias correction coefficient *k* between zircon (91500) and garnet (Willsboro, Mali and QC04) obtained from various spot sizes, integration intervals and repetition rates (A and B) as well as from the line scanning (C). Note that different materials show similar *k* values under the line scanning mode.

Where $\frac{C_{std}^{206Pb}}{C_{std}^{238U}}$ and $\frac{I_{std}^{206Pb}}{I_{std}^{238U}}$ represent the reference isotope concentration ratio and the measured isotope intensity ratio of the standard, respectively. Based on calculating the *k*, it is easy to find out the difference in U and Pb behaviors between the zircon and garnet and thus figure out the optimal conditions for the garnet U—Pb dating. The results of this study show that the zircon and garnet reference materials have enhanced difference in *k* at the high repetition rates while the *k* values of them are more consistent at the low repetition rates (Fig. 11A and B). This is in good agreement with our observations that the accurate ages of all the garnets can be favorably obtained at the relatively low repetition rates

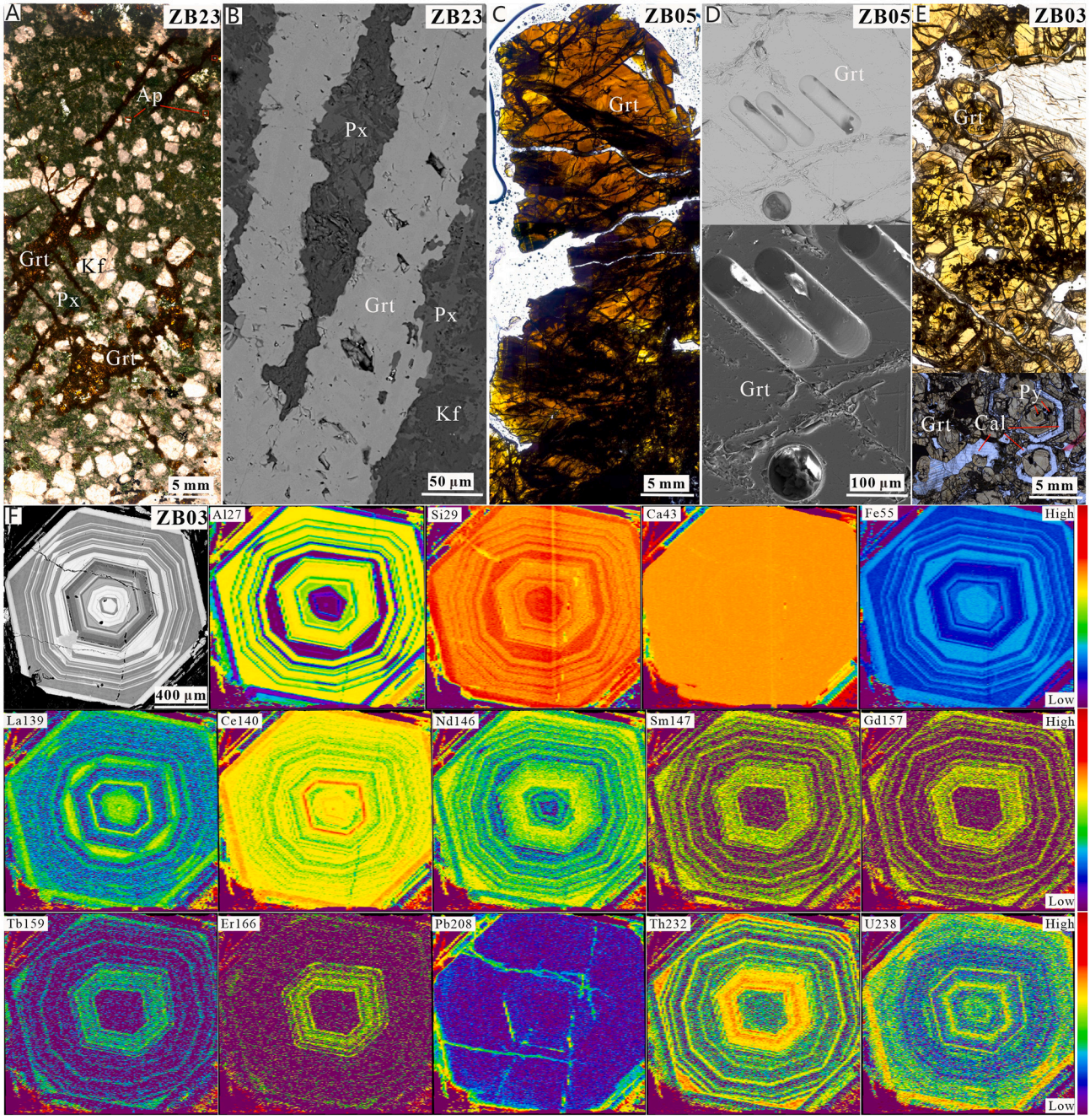

Fig. 12. The petrographic and elemental distribution characteristics of the garnets from the Jinling Fe skarn deposit. A, C and D were obtained from transmitted light under polarization microscope. B, D and F were obtained from BSE imaging under SEM. The elemental distribution of a zoned garnet grain (F) was obtained from LA-ICP-MS mapping. Abbreviations: Ap = Apatite; Cal = Calcite; Grt = Garnet; Kf = Potassic feldspar, Py = Pyrite; Px = Pyroxene.

(Figs. 7 and 9). In addition, under the line scanning mode, the *k* values of different materials are quite consistent and constant over time (Fig. 11C), corroborating the finding that line scanning works well for U—Pb dating under both the matrix-matched and non-matrix-matched conditions (Fig. 10).

Furthermore, it is noted that choosing different integration intervals has significant effect on the *k* value, especially for the zircon 91500 (Fig. 11B). Similar *k* values for both the zircon and garnet can be achieved if appropriate integration intervals (30 s) are selected. This implies that analyte signals should be chosen as consistent as possible between the sample and the standard in order to eliminate the time/depth-dependent U—Pb fractionation.

5. Applications

The above optimized methods were applied to various grandite garnets selected from the Jinling Fe, Xintianling W and Hongshan Cu—Mo skarn deposits. The characteristics of the garnets are summarized in Table 1 and the U—Pb isotopic data are listed in Supplementary Data.

5.1. Fe skarn deposit

There are three types of garnets developed in the Jinling Fe skarn deposit, which show compositions of $Ad_{72}Gr_{28}$ (ZB23), $Ad_{94}Gr_{6}$ (ZB05) and $Ad_{53\text{-}98}Gr_{2-47}$ (ZB03), respectively. From ZB23 to ZB05 and then to

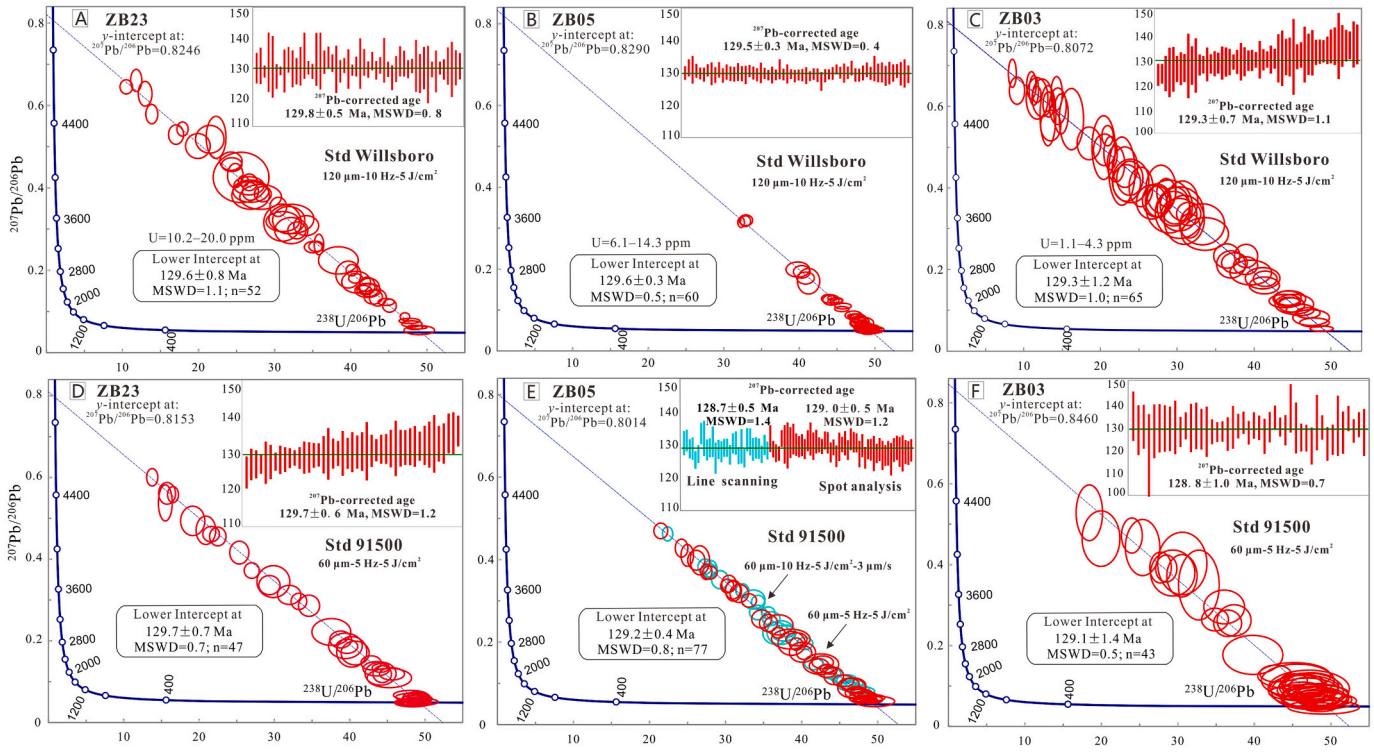

Fig. 13. Tera-Wasserburg Concordia diagrams and ^{207}Pb-corrected weighted mean $^{206}Pb/^{238}U$ ages of the garnets from the Jinling Fe skarn deposit, obtained from matrix-matched (A–C) and non-matrix-matched (D—F) conditions, respectively. Line scanning was also applied to the ZB05 (E).

ZB03, the U concentrations show a continuous decrease from 10.2–20.0 ppm (mean of 14.4 ppm) to 6.1–14.3 ppm (mean of 9.6 ppm) and then to 1.1–4.3 ppm (mean of 2.6 ppm). The ZB23 occurs as veinlet in the altered quartz monzonite, showing dark red color without chemical zoning (Fig. 12A and B). The ZB05 is from the exoskarn zone and featured by almost end-member andradite composition. It is red to brown and coarse-grained without significant zoning (Fig. 12C and D). The ZB03 is also from the exoskarn zone, showing light yellow color with remarkable chemical zoning (e.g., Si, Al, Fe) (Fig. 12E). The LA-ICP-MS elemental mapping of one zoned garnet grain from the ZB03 shows that U is either positively correlated with Al + Si + REE in the core or with Fe + Si + REE in the rim (Fig. 12F), supporting the consideration that U incorporation into the grandite garnets is mainly controlled by the coupled substitution of $[Ca^{2+}]^{VII}_{-1}[REE^{3+}, U^{4+}]^{VII}_{+1}[Si^{4+}]^{IV}_{-1}[Fe^{3+}, Al^{3+}]^{IV}_{+1}$ (Gaspar et al., 2008; Deng et al., 2017). The garnet grains of ZB03 are intergrown with magnetite and thus can directly constrain the timing of the Fe mineralization.

When using Willsboro as the external standard at the ablation parameters of 120 μm, 10 Hz and 5 J/cm^2, all the above garnets can be well dated. Fifty-two analyses from the ZB23 yield a Tera-Wasserburg Concordia lower intercept age of 129.6 ± 0.8 Ma (MSWD = 1.1) and a weighted mean ^{207}Pb-corrected $^{206}Pb/^{238}U$ age of 129.8 ± 0.5 Ma (MSWD = 0.8) (Fig. 13A). Sixty analyses from the ZB05 yield a Tera-Wasserburg Concordia lower intercept age of 129.6 ± 0.3 Ma (MSWD = 0.5) and a weighted mean ^{207}Pb-corrected $^{206}Pb/^{238}U$ age of 129.5 ± 0.3 Ma (MSWD = 0.4) (Fig. 13B). Sixty-five analyses from the ZB03 yield a Tera-Wasserburg Concordia lower intercept age of 129.3 ± 1.2 Ma (MSWD = 1.0) and a weighted mean ^{207}Pb-corrected $^{206}Pb/^{238}U$ age of 129.3 ± 0.7 Ma (MSWD = 1.1) (Fig. 13C). These ages are consistent with each other within errors.

When using zircon 91500 as the external standard at the ablation parameters of 60 μm, 5 Hz and 5 J/cm^2, the ZB23 yields a Tera-Wasserburg Concordia lower intercept age of 129.7 ± 0.7 Ma (MSWD = 0.7, n = 47) and a weighted mean ^{207}Pb-corrected $^{206}Pb/^{238}U$ age of 129.7 ± 0.6 Ma (MSWD = 1.2) (Fig. 13D). The ZB05 yields a Tera-Wasserburg Concordia lower intercept age of 129.2 ± 0.4 Ma (MSWD = 0.8, n = 77) and a weighted mean ^{207}Pb-corrected $^{206}Pb/^{238}U$ age of 129.0 ± 0.5 Ma (MSWD = 1.2) (Fig. 13E). The ZB03 yields a Tera-Wasserburg Concordia lower intercept age of 129.1 ± 1.4 Ma (MSWD = 0.5, n = 43) and a weighted mean ^{207}Pb-corrected $^{206}Pb/^{238}U$ age of 128.8 ± 1.0 Ma (MSWD = 0.7) (Fig. 13F). Line scanning was also applied to the ZB05 using zircon 91500 as external standard. At the scanning parameters of 60 μm, 10 Hz, 5 J/cm^2 and scanning speed of 3 μm/s, a weighted mean ^{207}Pb-corrected $^{206}Pb/^{238}U$ age of 128.7 ± 0.5 Ma (MSWD = 1.4, n = 30) was obtained (Fig. 13E).

The above results show that the U—Pb ages are quite consistent regardless of using zircon or garnet as the external standard, or using spot analysis or line scanning mode. All the ages are in good agreement with the LA-ICP-MS zircon $^{206}Pb/^{238}U$ age of the ore-forming quartz monzonite (129.7 ± 0.8 Ma, Lan et al., 2019). It is noteworthy the strongly zoned garnet can be precisely dated despite its widely varied compositions.

5.2. W skarn deposit

Two types of garnets occur in the Xintianling W skarn deposit, of which the first type (XTL01) shows obvious zoning (Fig. 14A and B) while the second (XTL02) does not (Fig. 14C and D). Both types contain high Mn contents, having a composition of $Ad_{31-75}Gr_{22-64}Sp_{2-6}$ (XTL01) and $Ad_{45-60}Gr_{34-47}Sp_{6-9}$ (XTL02), respectively. The garnet grains show higher Mn contents in the XTL02 than in the XTL01 with similar U concentrations (3.2–21.6 ppm). Spot analysis was applied to the XTL01 while line scanning was applied to the XTL02 since the latter is more homogeneous in composition and texture (Fig. 14C and D).

For the XTL01, using Willsboro as the external standard at the ablation parameters of 120 μm, 10 Hz and 5 J/cm^2, one hundred and ten analyses yield a Tera-Wasserburg Concordia lower intercept age of 158.2 ± 0.5 Ma (MSWD = 1.3) and a weighted mean ^{207}Pb-corrected $^{206}Pb/^{238}U$ age of 158.3 ± 0.3 Ma (MSWD = 0.8) (Fig. 14E). For the XTL02, at the scanning parameters of 60 μm, 10 Hz, 5 J/cm^2 and 3 μm/s,

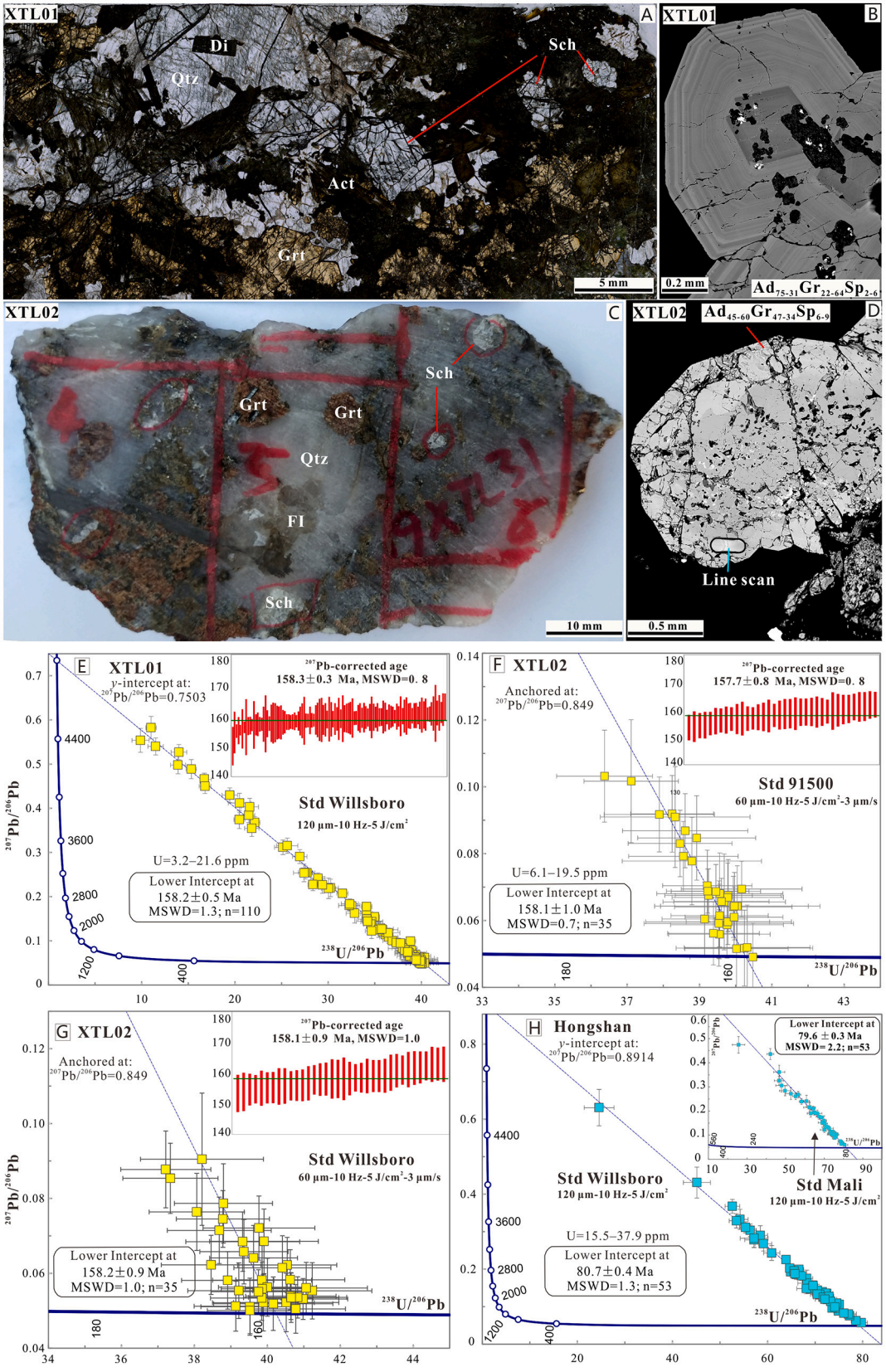

Fig. 14. Petrographic characteristics (A–D), Tera-Wasserburg Concordia diagrams and ^{207}Pb-corrected weighted mean $^{206}Pb/^{238}U$ ages (E–H) of the garnets from the Xintianling W and Hongshan Cu—Mo skarn deposits. A and C were obtained under transmitted light, while B and D were obtained from BSE imaging. Line scanning was applied to the XTL02 using 91500 (F) and Willsboro (G) as the external standards, respectively. Abbreviations: Qtz = Quartz; Di = Diopside; Act = Actinolite; FI=Fluorite; Sch = Scheelite.

thirty-five analyses yield a Tera-Wasserburg Concordia lower intercept age of 158.1 ± 1.0 Ma (MSWD = 0.7) and a weighted mean ^{207}Pb-corrected ^{206}Pb/^{238}U age of 157.7 ± 0.8 Ma (MSWD = 0.8) when using zircon 91500 as the external standard (Fig. 14F). If using Willsboro as the external standard, the above ages are 158.2 ± 0.9 Ma (MSWD = 1.0) and 158.1 ± 0.9 Ma (MSWD = 1.0), respectively (Fig. 14G).

Previous studies showed that the molybdenite *Re*—Os age of skarn ores is 159.1 ± 1.9 Ma (Yuan et al., 2012), the mica Ar—Ar age is 157.3 ± 1.0 Ma (Mao et al., 2004; Cai et al., 2008; Peng et al., 2007) and the Rb—Sr age of fluid inclusions is 157.4 ± 3.2 Ma (Cai et al., 2008). The U—Pb ages obtained from garnets in this study are in good agreement with the above ages, but have better precision.

5.3. Cu—Mo skarn deposit

The garnet from the Hongshan Cu—Mo deposit is dark red with a composition of $And_{40-61}Grs_{37-57}$. It contains higher U concentrations (15.5–37.9 ppm) than those of the garnets from the above two deposits. The Willsboro and Mali were used as the external standard at the ablation conditions of 120 μm, 10 Hz and 5 J/cm^2, respectively. When using the Willsboro as the external standard, fifty-three analyses yield a Tera-Wasserburg Concordia lower intercept U—Pb age of 80.7 ± 0.4 Ma (MSWD = 1.3) (Fig. 14H). A similar but slightly younger age of 79.6 ± 0.3 Ma (MSWD = 2.2) was obtained when using the Mali as the external standard (Fig. 14H). These ages are consistent with the molybdenite Re—Os ages (78.6–83.8 Ma) of the skarn ores (Meng et al., 2013; Wang et al., 2014) and the LA-ICP-MS zircon U—Pb age (81.1 ± 0.5 Ma) of the related granitic porphyry (Wang et al., 2011).

5.4. Prospects for application

The selected garnets from different deposits have compositions varying widely between andradite and grossular with variable U concentrations (from 1 to 100 ppm). To assess the effects of common Pb, the f_{206} values of them were calculated. It shows that the f_{206} values change from 0 to 0.73, variations of which are beyond 0.5 even in a single grain (Supplementary Data). This indicates that the amounts of common Pb in the garnets are quite variable and inhomogeneous, which seem to have little effect on the U—Pb ages when using the optimized methods in this study. In addition, according to the Tera-Waserburg plot, the obtained *y*-intercept ^{207}Pb/^{206}Pb ratios of garnets are 0.8014–0.8460 from the Jinling Fe deposit, 0.7503–0.849 from the Xintianling W deposit and 0.8914 from the Hongshan Cu—Mo deposit. The *y*-intercept ^{207}Pb/^{206}U ratios from the Jinling and Hongshan deposits are close to the terrestrial Pb isotope model (^{207}Pb/^{206}Pb of 0.84–0.85), but those of the Xintianling deposit vary widely. This indicates that some abnormal common Pb might be involved into the Xintianling garnets. Nonetheless, these garnets can be accurately dated. It is therefore promising that despite the complex compositions and variable U and Pb contents in natural garnets, they can be precisely dated just by adjusting the ablation parameters under either matrix-matched or non-matrix-matched condition. However, as mentioned before, because the low-U and high-U samples show contrasted behaviors in U—Pb fractionation during laser ablation, it is best to use U concentration-matched external standard for calibration, and thus it is necessary to evaluate the U concentrations of the garnet samples before U—Pb dating.

6. Conclusions

Based on the detailed experiments on ablation behaviors of U and Pb as well as the U—Pb age calibrations for different garnet samples under both the matrix-matched (garnet as external standard) and non-matrix-matched (zircon 91500 as external standard) conditions, the following conclusions can be drawn out:

(1) At least three types of U—Pb fractionation, which are associated with downhole depth, intrinsic properties of U (more refractory) and Pb (more volatile) and radiation damage (alpha dose) of crystal lattice, respectively, likely occur in zircon and garnet. The U—Pb fractionation can be minimized or even eliminated by optimizing the ablation parameters (e.g., large spot size and low repetition rate) or analytical modes (e.g., line scanning), making it feasible to use zircon as external standard for garnet U—Pb dating.
(2) Line scanning is the most favorable analytical way for garnet U—Pb dating under both the matrix-matched and non-matrix-matched conditions.
(3) In spot analysis mode, precise dating of garnets can be achieved under both the matrix-matched and non-matrix-matched conditions, but requires different ablation parameters. Large spot sizes (e.g., ≥90 μm) coupled with moderate repetition rate (e.g., 5 J/cm^2) and fluence (e.g., 5 J/cm^2) are favored for all the garnets, but the low-U (<10 ppm U) and high-U garnets (tens to hundreds of ppm U) are best treated differently.
(4) Natural garnets having widely varied compositions (from andradite to grossular) and variable U (e.g., 1–100 ppm) and common Pb (e.g., f_{206} = 0–70%) concentrations can be precisely dated by using the optimized methods, indicating that the methods are reliable and thus favorable for wide applications.
(5) In order to improve the accuracy and precision of garnet U—Pb dating, U-concentration matched garnet standards are required. It is necessary to develop moderate- to high-U garnet standards.

Declaration of Competing Interest

The authors declare that they have no known competing financial interests or personal relationships that could have appeared to influence the work reported in this paper.

Acknowledgements

We are grateful to S. Seman and Xiaodong Deng for providing the garnet reference materials. We thank Jianfeng Gao and Zhihui Dai for advice and help during LA-ICP-MS analysis, Wenqin Zheng and Xiang Li for EPMA analysis, Shaohua Dong and Xifeng Mi for SEM analysis. Three anonymous reviewers and the editor-in chief are also thanked for their constructive and critical comments. This study is financially supported by the National Key Research and Development Program of China (Grant No. 2018YFA0702603) and the Natural Science Foundation of China (Grant No. 41930430 and 41472079).

Appendix A. Supplementary data

The LA-ICP-MS U-Pb data of zircon and garnets obtained from various ablation conditions. Supplementary data to this article can be found online at https://doi.org/10.1016/j.chemgeo.2021.120198.

References

Aleinikoff, J.N., Wintsch, R.P., Fanning, C.M., Dorais, M.J., 2002. U-Pb geochronology of zircon and polygenetic titanite from the Glastonbury Complex, Connecticut, USA: an integrated SEM, EMPA, TIMS, and SHRIMP study. Chem. Geol. 188, 125–147.
Allen, C.M., Campbell, I.H., 2012. Identification and elimination of a matrix-induced systematic error in LA-ICP-MS ^{206}Pb/^{238}U dating of zircon. Chem. Geol. 332, 157–165.
Barrie, C.T., 1990. U-Pb garnet and titanite age for the Bristol Town-ship lamprophyre suite, western Abitibi Subprovince, Canada. Can. J. Earth Sci. 27, 1451–1456.
Bineli Betsi, T., Mokane, L., McFarlane, C., Phili, K., Kelepile, T., 2020. Multistage gold mineralization events in the Archean Tati Greenstone Belt, Northeast Botswana: constraints from integrative white mica Ar/Ar, garnet U-Pb and sulfides Pb/Pb geochronology. Precambrian Res. 2020 https://doi.org/10.1016/j.precamres.2020.105623.

Burisch, M., Gerdes, A., Meiner, L.D., Albert, R., Seifert, T., Gutzmer, J., 2019. The essence of time-fertile skarn formation in the Variscan Orogenic Belt. Earth Planet. Sci. Lett. 519, 165–170.
Burn, M., Lanari, P., Pettke, T., Engi, M., 2017. Non-matrix-matched standardisation in LA-ICP-MS analysis: general approach, and application to allanite Th-U-Pb dating. J. Anal. At. Spectrom. 32, 1359–1377.
Cai, M.H., Han, F.B., He, L.Q., Liu, G.Q., Chen, K.X., Fu, J.M., 2008. He, Ar isotope characteristics and Rb-Sr dating of the xintianling skarn scheelite deposit in Southern Hunan, China. Acta Geosci. Sin. 29, 167–173 (in Chinese with English abstracts).
Cheng, H., Vervoort, J.D., Dragovic, B., Wilford, D., Zhang, L., 2018. Coupled Lu-Hf and Sm-Nd geochronology on a single eclogitic garnet from the Huwan shear zone, China. Chem. Geol. 476, 208–222.
Chew, D.M., Sylvester, P.J., Tubrett, M.N., 2011. U–Pb and Th–Pb dating of apatite by LA-ICPMS. Chem. Geol. 280, 200–216.
Chew, D.M., Petrus, J.A., Kamber, B.S., 2014. U-Pb LA-ICPMS dating using accessory mineral standards with variable common Pb. Chem. Geol. 363, 185–199.
Darling, J.R., Storey, C.D., Engi, M., 2012. Allanite U-Th-Pb geochronology by laser ablation ICPMS. Chem. Geol. 292, 103–115.
Deng, X.D., Li, J.W., Luo, T., Wang, H.Q., 2017. Dating magmatic and hydrothermal processes using andradite-rich garnet U-Pb geochronometry. Contrib. Mineral. Petrol. 172, 71.
Eggins, S.M., Kinsley, L.P.J., Shelley, J.M.M., 1998. Depositionand element fractionation processes during atmospheric pressure laser sampling for analysis by ICPMS. Appl. Surf. Sci. 127-129, 278–286.
El Korh, A., 2014. Ablation behaviour of allanites during U-Th-Pb dating using a quadrupole ICP-MS coupled to a 193 nm excimer laser. Chem. Geol. 371, 46–59.
Fan, G.H., Li, J.W., Deng, X.D., Gao, W.S., Li, S.Y., 2021. Age and Origin of the Dongping Au-Te Deposit in the North China Craton Revisited: Evidence from Paragenesis, Geochemistry, and In Situ U-Pb Geochronology of Garnet. Economic Geology. https://doi.org/10.5382/econgeo.4810.
Fietzke, J., Frische, M., 2016. Experimental evaluation of elemental behavior during LA-ICP-MS: influences of plasma conditions and limits of plasma robustness. J. Anal. At. Spectrom. 31, 234–244.
Fryer, B.J., Jackson, S.E., Longerich, H.P., 1995. Design, operation and role of the laser ablation coupled with an inductively coupled plasma mass spectrometer (LAM-ICP-MS) in the Earth Sciences. Can. Mineral. 33, 303–312.
Garcia, C.C., Lindner, H., Niemax, K., 2007. Transport efficiency in femtosecond laser ablation inductively coupled plasma mass spectrometry applying ablation cells with short and long washout times. Spectrochim. Acta B-Atom. Spectrosc. 62, 13–19.
Gaspar, M., Knaack, C., Meinert, L.D., Moretti, R., 2008. REE in skarn systems: a LA-ICP-MS study of garnets from the Crown Jewel gold deposit. Geochim. Cosmochim. Acta 72, 185–205.
Gevedon, M., Seman, S., Barnes, J.D., Lackey, J.S., Stockli, D.F., 2018. Unraveling histories of hydrothermal systems via U-Pb laser ablation dating of skarn garnet. Earth Planet. Sci. Lett. 498, 237–246.
Gregory, C.J., Rubatto, D., Allen, C.M., Williams, I.S., Hermann, J., Ireland, T., 2007. Allanite micro-geochronology: a LA-ICP-MS and SHRIMP U-Th-Pb study. Chem. Geol. 245, 162–182.
Guillong, M., Kuhn, H.R., Günther, D., 2003. Application of a particle separation device to reduce inductively coupled plasma-enhanced elemental fractionation in laser ablation-inductively coupled plasma-mass spectrometry. Spectrochim. Acta B-Atom. Spectrosc. 58, 211–220.
Günther, D., Hattendorf, B., 2005. Solid sample analysis using laser ablation inductively coupled plasma mass spectrometry. Trac-Trends Analyt. Chem. 24, 255–265.
Hirata, T., 1997. Soft ablation technique for laser ablation-induc-tively coupled plasma mass-spectrometry. J. Anal. At. Spectrom. 12, 1337–1342.
Hirata, T., Nesbitt, R.W., 1995. U-Pb isotope geochronology of zircon: evaluation of the laser probe-inductively coupled plasma mass spectrometry technique. Geochim. Cosmochim. Acta 59, 2491–2500.
Horn, I., Rudnick, R.L., McDonough, W.F., 2000. Precise elemental and isotope ratio determination by simultaneous solution nebulization and laser ablation-ICP-MS: application to U-Pb geochronology. Chem. Geol. 164, 281–301.
Hu, Z.C., Gao, S., Liu, Y.S., Hu, S.H., Chen, H.H., Yuan, H.L., 2008. Signal enhancement in laser ablation ICP-MS by addition of nitrogen in the central channel gas. J. Anal. At. Spectrom. 23, 1093–1101.
Huggins, F.E., Virgo, D., Huckenholz, H.G., 1977. Titanium-containing silicate garnets. II. The crystal chemistry of melanites and schorlomites. Am. Mineral. 62, 646–665.
Jung, S., Mezger, K., 2003. U-Pb garnet chronometry in high-grade rocks-case studies from the Central Damara orogen (Namibia) and implications for the interpretation of Sm-Nd garnet ages and the role of high U-Th inclusions. Contrib. Mineral. Petrol. 146, 382–396.
Jung, S., Brandt, S., Bast, R., Scherer, E.E., Berndt, J., 2019. Metamorphic petrology of a high-T/low-P granulite terrane (Damara belt, Namibia)-Constraints from pseudosection modelling and high-precision Lu-Hf garnet-whole rock dating. J. Metamorph. Geol. 37, 41–69.
Koch, J., Von Bohlen, A., Hergenroder, R., Niemax, K., 2004. Particle size distributions and compositions of aerosols produced by near-IR femto- and nanosecond laser ablation of brass. J. Anal. At. Spectrom. 19, 267–272.
Košler, J., Wiedenbeck, M., Wirth, R., Hovorka, J., Sylvester, P., Mikova, J., 2005. Chemical and phase composition of particles produced by laser ablation of silicate glass and zircon-implications for elemental fractionation during ICP-MS analysis. J. Anal. At. Spectrom. 20, 402–409.
Kuhn, H.R., Guillong, M., Günther, D., 2004. Size-related vaporisation and ionisation of laser-induced glass particles in the inductively coupled plasma. Anal. Bioanal. Chem. 378, 1069–1074.
Lan, T.G., Hu, R.Z., Chen, Y.H., Wang, H., Tang, Y.W., Liu, L., 2019. Generation of high-Mg diorites and associated iron mineralization within an intracontinental setting: Insights from ore-barren and ore-bearing intrusions in the eastern North China Craton. Gondwana Res. 72, 97–119.
Li, X.H., Liang, X.R., Sun, M., Guan, H., Malpas, J.G., 2001. Precise Pb^{206}/U^{238} age determination on zircons by laser ablation microprobe-inductively coupled plasma-mass spectrometry using continuous linear ablation. Chem. Geol. 175, 209–219.
Li, J.W., Deng, X.D., Zhou, M.F., Liu, Y.S., Zhao, X.F., Guo, J.L., 2010. Laser ablation ICP-MS titanite U-Th-Pb dating of hydrothermal ore deposits: a case study of the Tonglushan Cu-Fe-Au skarn deposit, SE Hubei Province, China. Chem. Geol. 270, 56–67.
Li, D.F., Fu, Y., Sun, X.M., 2018. Onset and duration of Zn-Pb mineralization in the Talate Pb-Zn (-Fe) skarn deposit, NW China: Constraints from spessartine U-Pb dating. Gondwana Res. 63, 117–128.
Liu, Y.S., Gao, S., Hu, Z.C., Gao, C.G., Zong, K.Q., Wang, D.B., 2010. Continental and oceanic crust recycling-induced melt-peridotite interactions in the Trans-North China Orogen: U-Pb dating, Hf isotopes and trace elements in zircons from Mantle xenoliths. J. Petrol. 51, 537–571.
Ludwig, K.R., 2003. User's Manual for Isoplot 3.00, a Geochronological Toolkit for Microsoft Excel. Berkeley Geochronological Center Special Publication, No. 4, pp. 25–32.
Luo, T., Hu, Z., Zhang, W., Liu, Y., Zong, K., Zhou, L., Zhang, J., Hu, S., 2018. Water vapor-assisted "universal" nonmatrix-matched analytical method for the in situ U-Pb dating of zircon, monazite, titanite, and xenotime by laser ablation-inductively coupled plasma mass spectrometry. Anal. Chem. 90, 9016–9024.
Luo, T., Deng, X.D., Li, J.W., Hu, Z.C., Zhang, W., Liu, Y.S., Zhang, J.F., 2019. U-Pb geochronology of wolframite by laser ablation inductively coupled plasma mass spectrometry. J. Anal. At. Spectrom. 34, 1439–1446.
Machida, R., Nakazawa, T., Sakuraba, Y., Fujiwara, M., Furuta, N., 2015. Particle size-related elemental fractionation in laser ablation in liquid inductively coupled plasma mass spectrometry. J. Anal. At. Spectrom. 30, 2412–2419.
Mank, A.J.G., Mason, P.R.D., 1999. A critical assessment of laser ablation ICP-MS as an analytical tool for depth analysis in silica-based glass samples. J. Anal. At. Spectrom. 14, 1143–1153.
Mao, J.W., Li, X.F., Chen, W., Lan, X.M., Wei, S.L., 2004. Geological characteristics of the Furong tin orefield, Hunan, Ar-Ar dating of tin ores and related granite and its geodynamic significance for rock and ore formation. Acta Geologica Sinica (English Edition) 78, 481–491.
Marillo-Sialer, E., Woodhead, J., Hanchar, J.M., Reddy, S.M., Greig, A., Hergt, J., Kohn, B., 2016. An investigation of the laser-induced zircon 'matrix effect'. Chem. Geol. 438, 11–24.
Meinert, L.D., Dipple, G.M., Nicolescu, S., 2005. World skarn deposits. Econ. Geol. 100, 299–336.
Meng, J.Y., Yang, L.Q., Lu, L., Gao, X., Li, J.X., Luo, Y.Z., 2013. Re-Os dating of molybdenite from the Hongshan Cu-Mo deposit in Northwest Yunnan and its implications for mineralization. Acta Petrol. Sin. 29, 1214–1222 (in Chinese with English abstracts).
Mezger, K., Hanson, G.N., Bohlen, S.R., 1989. U-Pb systematics of garnet: dating the growth of garnet in the late Archean Pikwitonei granulite domain at Cauchon and Natawahunan Lakes, Manitoba, Canada. Contrib. Mineral. Petrol. 101, 136–148.
Outridge, P.M., Doherty, W., Gregoire, D.C., 1997. Ablative and transport fractionation of trace elements during laser sampling of glass and copper. Spectrochim. Acta B-Atom. Spectrosc. 52, 2093–2102.
Paton, C., Hellstrom, J., Paul, B., Woodhead, J., Hergt, J., 2011. Iolite: Freeware for the visualisation and processing of mass spectrometric data. J. Anal. At. Spectrom. 26, 2508–2518.
Peng, J.T., Hu, R.Z., Bi, X.W., Dai, D.M., Li, Z.L., Li, X.M., Yan, S., Yuan, S.D., Liu, S.R., 2007. Ar-Ar isotopic dating of tin mineralization in Furong deposit of Hunan Province and its geological significance. Mineral Deposits 26, 237–248 (in Chinese with English abstract).
Poitrasson, F., Mao, X.L., Mao, S.S., Freydier, R., Russo, R.E., 2003. Comparison of ultraviolet femtosecond and nanosecond laser ablation inductively coupled plasma mass spectrometry analysis in glass, monazite, and zircon. Anal. Chem. 75, 6184–6190.
Python, M., Ceuleneer, G., Ishida, Y., Barrat, J.A., Arai, S., 2007. Oman diopsidites: a new lithology diagnostic of very high temperature hydrothermal circulation in mantle peridotite below oceanic spreading centres. Earth Planet. Sci. Lett. 255, 289–305.
Romer, R.L., Siegesmund, S., 2003. Why allanite may swindle about its true age. Contrib. Mineral. Petrol. 146, 297–307.
Scheibner, B., Wörner, G., Civetta, L., Stosch, H.G., Simon, K., Kronz, A., 2007. Rare earth element fractionation in magmatic Ca-rich garnets. Contrib. Mineral. Petrol. 154, 55–74.
Scherer, E.E., Cameron, K.L., Blichert-Toft, J., 2000. Lu-Hf garnet geochronology: Closure temperature relative to the Sm-Nd system and the effects of trace mineral inclusions. Geochim. Cosmochim. Acta 64, 3413–3432.
Seman, S., Stockli, D.F., McLean, N.M., 2017. U-Pb geochronology of grossular-andradite garnet. Chem. Geol. 460, 106–116.
Shaheen, M.E., Gagnon, J.E., Fryer, B.J., 2012. Femtosecond (fs) lasers coupled with modern ICP-MS instruments provide new and improved potential for in situ elemental and isotopic analyses in the geosciences. Chem. Geol. 330, 260–273.
Sliwinski, J.T., Guillong, M., Liebske, C., Dunkl, I., Von Quadt, A., Bachmann, O., 2017. Improved accuracy of LA-ICP-MS U-Pb ages of Cenozoic zircons by alpha dose correction. Chem. Geol. 472, 8–21.
Smit, M.A., Scherer, E.E., Mezger, K., 2013. Lu-Hf and Sm-Nd garnet geochronology: chronometric closure and implications for dating petrological processes. Earth Planet. Sci. Lett. 381, 222–233.

Smith, M.P., Henderson, P., Jeffries, T.E.R., Long, J., Williams, C.T., 2004. The rare earth elements and uranium in garnets from the Beinn an Dubhaich aureole, Skye, Scotland, UK: Constraints on processes in a dynamic hydrothermal system. J. Petrol. 45, 457–484.
Stacey, J.S., Kramers, J.D., 1975. Approximation of terrestrial lead isotope evolution by a two-stage model. Earth Planet. Sci. Lett. 26, 207–226.
Steely, A.N., Hourigan, J.K., Juel, E., 2014. Discrete multi-pulse laser ablation depth profiling with a single-collector ICP-MS: Sub-micron U-Pb geochronology of zircon and the effect of radiation damage on depth-dependent fractionation. Chem. Geol. 372, 92–108.
Storey, C.D., Jeffries, T.E., Smith, M., 2006. Common lead-corrected laser ablation ICP-MS U-Pb systematics and geochronology of titanite. Chem. Geol. 227, 37–52.
Tera, F., Wasserburg, G.J., 1972. U-Th-Pb systematics in three Apollo 14 basalts and the problem of initial Pb in lunar rocks. Earth Planet. Sci. Lett. 14, 281–304.
Thompson, J.M., Meffre, S., Danyushevsky, L., 2018. Impact of air, laser pulse width and fluence on U-Pb dating of zircons by LA-ICPMS. J. Anal. At. Spectrom. 33, 221–230.
Tian, Z.D., Leng, C.B., Zhang, X.C., Zafar, T., Zhang, L.J., Hong, W., Lai, C.K., 2019. Chemical composition, genesis and exploration implication of garnet from the Hongshan Cu-Mo skarn deposit, SW China. Ore Geol. Rev. 112, 103016.
Ulianov, A., Muentener, O., Schaltegger, U., Bussy, F., 2012. The data treatment dependent variability of U-Pb zircon ages obtained using mono-collector, sector field, laser ablation ICPMS. J. Anal. At. Spectrom. 27, 663–676.
Ulrich, T., Kamber, B.S., Jugo, P.J., Tinkham, D.K., 2009. Imaging element distribution patterns in minerals by laser ablation-inductively coupled plasma-mass spectrometry (LA-ICP-MS). Can. Mineral. 47, 1001–1012.
Wafforn, S., Seman, S., Kyle, J.R., Stockli, D., Leys, C., Sonbait, D., Cloos, M., 2018. Andradite garnet U-Pb geochronology of the big Gossan skarn, Ertsberg-Grasberg mining district, Indonesia. Econ. Geol. 113, 769–778.
Wang, X.S., Bi, X.W., Leng, C.B., Tang, Y.Y., Lan, J.B., Qi, Y.Q., Shen, N.P., 2011. LA-ICP-MS Zircon U-Pb dating of granite porphyry in then Hongshan Cu-polymetallic deposit, Zhongdian, Northwest Yunnan, China and its geological implication. Acta Mineral. Sin. 31, 315–321 (in Chinese with English abstracts).
Wang, X.S., Bi, X.W., Leng, C.B., Zhong, H., Tang, H.F., Chen, Y.W., Yin, G.H., Huang, D. Z., Zhou, M.F., 2014. Geochronology and geochemistry of Late Cretaceous igneous intrusions and Mo-Cu-(W) mineralization in the southern Yidun Arc, SW China: Implications for metallogenesis and geodynamic setting. Ore Geol. Rev. 61, 73–95.
Wiedenbeck, M., Hanchar, J.M., Peck, W.H., Sylvester, P., Valley, J., Whitehouse, M., Kronz, A., Morishita, Y., Nasdala, L., Fiebig, J., Franchi, I., Girard, J.P., Greenwood, R.C., Hinton, R., Kita, N., Mason, P.R.D., Norman, M., Ogasawara, M., Piccoli, R., Rhede, D., Satoh, H., Schulz-Dobrick, B., Skar, O., Spicuzza, M.J., Terada, K., Tindle, A., Togashi, S., Vennemann, T., Xie, Q., Zheng, Y.F., 2004. Further characterisation of the 91500 zircon crystal. Geostand. Geoanal. Res. 28, 9–39.
Williams, I.S., 1998. U-Th-Pb geochronology by ion microprobe. In: McKibben, M.A., Shanks III, W.C., Ridley, W.I. (Eds.), Applications of Microanalytical Techniques to Understanding Mineralizing Processes, Reviews in Economic Geology, vol. 7, pp. 1–35.
Xu, J., Ciobanu, C.L., Cook, N.J., Zheng, Y., Sun, X., Wade, B.P., 2016. Skarn formation and trace elements in garnet and associated minerals from Zhibula copper deposit, Gangdese Belt, southern Tibet. Lithos 262, 213–231.
Yan, S., Zhou, R.J., Niu, H.C., Feng, Y.X., Nguyen, A.D., Zhao, Z.H., Yang, W.B., Qian, D., Zhao, J.X., 2020. LA-MC-ICP-MS U-Pb dating of low-U garnets reveals multiple episodes of skarn formation in the volcanic-hosted iron mineralization system, Awulale belt, Central Asia. GSA Bull. 132, 1031–1045.
Yang, L.Q., Deng, J., Dilek, Y., Meng, J.Y., Gao, X., Santosh, M., Wang, D., Yan, H., 2016. Melt source and evolution of I-type granitoids in the SE Tibetan Plateau: Late Cretaceous magmatism and mineralization driven by collision-induced transtensional tectonics. Lithos 245, 258–273.
Yang, Y.H., Wu, F.Y., Yang, J.H., Mitchell, R.H., Zhao, Z.F., Xie, L.W., Huang, C., Ma, Q., Yang, M., Zhao, H., 2018. U-Pb age determination of schorlomite garnet by laser ablation inductively coupled plasma mass spectrometry. J. Anal. At. Spectrom. 33, 231–239.
Yuan, S.D., Zhang, D.L., Shuang, Y., Du, A.D., Qu, W.J., 2012. Re-Os dating of molybdenite from the Xintianling giant tungsten-molybdenum deposit in southern Hunan Province, China and its geological implications. Acta Petrol. Sin. 28, 27–38 (in Chinese with English abstracts).
Zhang, S.T., Chen, H.Y., Shu, Q.H., Zhang, Y., Chu, G.B., Cheng, J.M., Tian, J., 2019. Unveiling growth histories of multi-generational garnet in a single skarn deposit via newly-developed LA-ICP-MS U-Pb dating of grandite. Gondwana Res. 73, 65–76.